

Implementation, Simulation and Evaluation of the Water Temperature in the Global Hydrological Model WaterGAP

Abschlussarbeit zur Erlangung des akademischen Grades
Master of Science (M.Sc.) Physische Geographie

an der Johann Wolfgang Goethe-Universität, Frankfurt am Main

vorgelegt von

Sebastian Ackermann

geb. am 05.09.1988 in Aschaffenburg

Erstgutachter: Dr. H. Müller Schmied

Zweitgutachterin: Prof. Dr. P. Döll

Eingereicht am 23. September 2020

Erklärung

Ich versichere hiermit, dass ich die vorliegende Arbeit selbstständig verfasst und keine anderen als die im Literaturverzeichnis angegebenen Quellen benutzt habe. Alle Stellen, die wörtlich oder sinngemäß aus veröffentlichten oder noch nicht veröffentlichten Quellen entnommen sind, sind als solche kenntlich gemacht. Die Zeichnungen oder Abbildungen in dieser Arbeit sind von mir selbst erstellt worden oder mit einem entsprechenden Quellennachweis versehen. Diese Arbeit ist in gleicher oder ähnlicher Form noch bei keiner anderen Stelle zur Prüfung eingereicht worden.

Mainz, den 23. September 2020

Sebastian Ackermann

Sebastian Ackermann

Zusammenfassung

WaterGAP (Water - Global Assessment and Prognosis) ist ein Werkzeug zur Modellierung des globalen Wasserverbrauchs und der Wasserverfügbarkeit. Es nimmt mit anderen Modellen an der ISIMIP Initiative (The Inter-Sectoral Impact Model Intercomparison Project) teil. Als Teil dieser Initiative soll die Wassertemperatur von teilnehmenden hydrologischen Modellen berechnet werden, da diese bei vielen chemischen, physikalischen und biologischen Prozessen eine wichtige Rolle spielt. Deshalb ist das Ziel dieser Masterarbeit, den Physik basierten Ansatz von VAN BEEK ET AL. (2012) und WANDERS ET AL. (2019) in WaterGAP zu integrieren und die Ergebnisse mit dem statistischen Regressionsmodell von PUNZET ET AL. (2012) zu vergleichen. Die Berechnung der Wassertemperatur wird mittels gemessener Temperaturdaten aus der GEMStat Wasserqualitätsdatenbank validiert. Die Ergebnisse sind gut für arktische und gemäßigte Breiten. Die Wassertemperaturen für Flüsse in tropischen Regionen werden überschätzt, was höchstwahrscheinlich auf die Überschätzung der Niederschlagstemperaturen, der einfallenden Strahlung und der Grundwassertemperaturen zurückzuführen ist. Der Vergleich mit dem Regressionsmodell von PUNZET ET AL. (2012) zeigt übereinstimmende Ergebnisse. Das Regressionsmodell stimmt sogar mit den WaterGAP Ergebnissen für die meisten Klimawandelszenarien überein, obwohl das Regressionsmodell aufgrund sich ändernder Umweltparameter nicht mehr funktionieren sollte. Für die Berechnung der Wassertemperatur durch WaterGAP mussten mehrere Annahmen getroffen werden. Dazu gehören z. B. Temperaturen für Kraftwerkskühlwasser sowie Niederschlags- und Oberflächenabflusstemperaturen. Für Modellverbesserungen könnten vielleicht drei verschiedene Werte für die verschiedenen Regionen der Welt zur Abkühlung des Niederschlags und des Oberflächenabflusses verwendet werden. Das Modell könnte auch durch eine Verfeinerung der Eisbildungsberechnung verbessert werden, insbesondere für die Bedingungen, unter denen das Eis schmilzt, aufbricht und stromabwärts transportiert wird. Darüber hinaus könnte die Rückkopplung auf die Kanalrauigkeit des Flusses implementiert werden, wenn sich Eis gebildet hat. Das um die Wassertemperaturberechnung verbesserte WaterGAP Modell wird die ISIMIP Initiative in Zukunft unterstützen können.

Abstract

WaterGAP (Water - Global Assessment and Prognosis) is a tool for modeling global water use and water availability. It participates among other models in the ISIMIP initiative (The Inter-Sectoral Impact Model Intercomparison Project). As part of this initiative, the water temperature should be calculated by participating hydrological models because it plays a vital role in many chemical, physical and biological processes. Therefore, the subject of this master thesis is to implement the physically based surface water temperature computation after VAN BEEK ET AL. (2012) and WANDERS ET AL. (2019) into WaterGAP and compare the results to the statistical regression approach by PUNZET ET AL. (2012). The computation is validated with observed water temperature data obtained from the GEMStat water quality database. The results are good for arctic and temperate latitudes. Surface water temperatures for tropical rivers are overestimated, most likely due to the overestimation of precipitation temperatures, incoming radiation and groundwater temperatures. The comparison with the regression model by PUNZET ET AL. (2012) shows matching results. The regression model even matches with WaterGAP results for most of the simulations of the future under climate change conditions, where the regression model should stop working due to changing environmental parameters. Several assumptions had to be made in order to implement the water temperature calculation in WaterGAP. These include, e.g., discharge temperatures for power plant cooling water, precipitation and surface runoff temperatures. For model improvements, perhaps three different values for the different regions of the world should be used to cool down the precipitation and surface runoff. The model could also be improved by refining the ice formation calculation, especially for the conditions when the ice melts, breaks up and is transported downstream. Furthermore, the feedback to the river channel roughness could be implemented if ice has formed. The WaterGAP model upgraded with the water temperature calculation will help the ISIMIP initiative in the future.

Acknowledgment

I would like to express my sincere gratitude to my advisor Dr. H. Müller-Schmied, for proposing the topic of this master thesis, and his support throughout the course of my thesis. I also would like to thank Prof. Dr. P. Döll for being my second supervisor. I also thank my father and friends for their moral support and fruitful discussions.

Table of Contents

| | |
|--|-------------|
| List of Figures | VIII |
| List of Tables | IX |
| 1 Introduction | 1 |
| 1.1 The State of Research | 1 |
| 1.1.1 Calculation of the Water Temperature: PUNZET ET AL. (2012) | 3 |
| 1.1.2 Calculation of the Water Temperature: VAN BEEK ET AL. (2012) | 4 |
| 2 Methodological Approach | 7 |
| 2.1 Implementation in WaterGAP | 7 |
| 2.2 Climate Forcing Data Used for WaterGAP Runs | 12 |
| 2.3 Data & Coefficients Used for Validation | 13 |
| 2.3.1 Observed Data | 13 |
| 2.3.2 Coefficients | 17 |
| 3 Evaluation and Validation | 18 |
| 3.1 Model Variations | 18 |
| 3.2 Standard Simulation Run | 19 |
| 3.3 Other Validation Runs | 24 |
| 3.3.1 Groundwater Variations | 24 |
| 3.3.2 Power Plant Cooling | 26 |
| 3.3.3 No Ice Formation | 27 |
| 3.3.4 No Water Use | 28 |
| 3.3.5 No Precipitation Cooling | 28 |
| 3.3.6 Natural Run | 28 |
| 3.3.7 No Reservoirs | 29 |
| 3.4 Sensitivity Analysis | 29 |
| 3.5 Simulation of the Future | 30 |
| 4 Discussion, Analysis and Interpretation of Results | 37 |
| 4.1 Influence of Observed Data Availability on Validation | 37 |
| 4.2 Standard Simulation Run | 40 |
| 4.3 Other Validation Runs | 41 |

| | | |
|----------|--|-----------|
| 4.3.1 | Groundwater Variations | 41 |
| 4.3.2 | Power Plant Cooling | 41 |
| 4.3.3 | No Ice Formation | 42 |
| 4.3.4 | No Water Use | 42 |
| 4.3.5 | No Precipitation Cooling | 43 |
| 4.3.6 | Natural Run | 43 |
| 4.3.7 | No Reservoir | 43 |
| 4.4 | Comparison of WaterGAP With the Regression Model of PUNZET ET AL. (2012) for Future Climate Scenarios | 44 |
| 5 | Conclusions and Prospects | 50 |
| | Bibliography | 51 |
| A | Appendix | 55 |
| A.1 | Structure of Folders | 55 |
| A.1.1 | Folder evaluations | 55 |
| A.1.2 | Folder model_data | 57 |
| A.1.3 | Folder R_scripts | 58 |
| A.1.4 | Folder validation_data | 58 |
| A.2 | Description of R Scripts | 58 |

List of Figures

| | | |
|-----|---|----|
| 1.1 | Schematic representation of the energy balance (VAN BEEK ET AL. 2012) | 5 |
| 2.1 | Flow of the water in WaterGAP | 7 |
| 2.2 | Corresponding water temperature calculation to the flow of the water in WaterGAP | 8 |
| 2.3 | Schematic representation of the energy balance WaterGAP | 10 |
| 2.4 | Cells with omitted river calculation | 11 |
| 2.5 | Worldwide selected measuring stations | 14 |
| 3.1 | Boxplots of the KGE, r , β and γ part 1 | 22 |
| 3.2 | Boxplots of the KGE, r , β and γ part 2 | 23 |
| 3.3 | Location of all measuring stations along the Rhine | 25 |
| 3.4 | Change of continental area with specific water temperature range due to climate change | 31 |
| 3.5 | Worldwide water temperature mean 1916-1990 | 32 |
| 3.6 | Worldwide water temperature mean 2071-2099 RCP2.6 | 33 |
| 3.7 | Worldwide water temperature mean 2071-2099 RCP4.5 | 34 |
| 3.8 | Worldwide water temperature mean 2071-2099 RCP6 | 35 |
| 3.9 | Worldwide water temperature mean 2071-2099 RCP8.5 | 36 |
| 4.1 | An example for an estuary downstream of a measuring station. | 38 |
| 4.2 | Surroundings of station AUS00004 | 41 |
| 4.3 | NLD00001 comparison of natural run, standard run and observed data | 44 |
| 4.4 | Comparison of future scenarios for WaterGAP and the regression model CHN00002 | 45 |
| 4.5 | Comparison of future scenarios for WaterGAP and the regression model NLD00001 | 46 |
| 4.6 | Comparison of future scenarios for WaterGAP and the regression model CAN00006 | 47 |
| 4.7 | Comparison of future scenarios for WaterGAP and the regression model RUS00011 | 48 |
| 4.8 | Comparison of future scenarios for WaterGAP and the regression model ARG00012 | 49 |

List of Tables

| | | |
|------|--|----|
| 1.1 | Regression parameters as results of the curve fitting by PUNZET ET AL. (2012) | 4 |
| 2.1 | Stations used for validation | 15 |
| 3.1 | Overview of computed scenarios for validation | 19 |
| 3.2 | Results standard simulation run | 19 |
| 3.3 | Worldwide median and average values of the NSE, KGE and RMSE | 21 |
| 3.4 | Results groundwater 4 °C | 24 |
| 3.5 | Results groundwater max. 25 °C | 26 |
| 3.6 | Results groundwater max. 25 °C at equator | 26 |
| 3.7 | Results power plant +10 °C | 27 |
| 3.8 | Results no power plant cooling | 27 |
| 3.9 | Results no ice build-up | 27 |
| 3.10 | Results without human use | 28 |
| 3.11 | Results precipitation not cooled down | 28 |
| 3.12 | Results natural run | 29 |
| 3.13 | Results no reservoirs | 29 |
| 3.14 | Sensitivity analysis | 30 |
| 3.15 | Change of continental area with specific water temperature range due to climate change | 31 |
| 4.1 | Comparison of DEU00006 and NLD00001 stations | 37 |
| 4.2 | Observed data for station DEU00006 | 39 |
| 4.3 | Observed data for station NLD00001 | 39 |
| 4.4 | Station AUS00004 scenario comparison | 40 |
| 4.5 | Station POL00006 scenario comparison | 42 |

1. Introduction

1.1. The State of Research

The modeling of global water use and water availability is essential, for example, for assessing current and future large-scale water problems, like trans-boundary groundwater use and overuse (HERBERT & DÖLL 2019). The not coordinated changes to the Tigris Euphrates system between the riparian states of Turkey, Iran, Syria and Iraq (JONES ET AL. 2008) are another example. These problems will increase in the future under the aspect of climate change. The global water availability and water use model WaterGAP (Water - Global Assessment and Prognosis) (DÖLL ET AL. 2003; MÜLLER SCHMIED ET AL. 2014) can be used as a tool for this purpose.

WaterGAP computes with the help of its submodel WGHM (WaterGAP Global Hydrology Model) water flows and water storages as well as human use of ground- and surface water (DÖLL ET AL. 2003). WaterGAP covers the global land area, including small islands and Greenland, but excluding Antarctica. For this, the WATCH-CRU land-sea-mask is used (MÜLLER SCHMIED ET AL. 2020). The model divides the land area into 67420 cells, representing a surface area of $0.5 \times 0.5^\circ$ each, which equals approximately 55×55 km at the equator. The continental grid cell area is defined as the cell area calculated with equal area cylindrical projection minus the ocean area, which is determined by the ESRI worldmask shapefile (MÜLLER SCHMIED ET AL. 2020). Every day, which is the standard timestep of WaterGAP, each cell's land area is recalculated, since all surface water bodies except rivers have a variable surface area, which is subtracted from the continental area. Rivers are an exception because exactly one river exists in every cell, but the surface area is not calculated. Every river has a length of 55 km, which is altered with a meandering ratio to account for meandering of the rivers. An example of river representation in WaterGAP can be seen in figure 3.3.

This hydrological model participates among others in the ISIMIP initiative (The Inter-Sectoral Impact Model Intercomparison Project, <https://www.isimip.org/>). ISIMIP is a modeling initiative with the aim of quantitatively representing the different cross-sectoral impacts of climate change and the associated uncertainties by offering a framework for cross-sectoral and cross-scale modeling. WaterGAP is one of the currently 13 models whose model results are made available to the global water sector of ISIMIP. However, until now, WaterGAP did not include the water temperature, although it plays an important role in many chemical, physical and biological processes (VAN VLIET ET AL. 2012).

Changes in water temperature, for example, due to climate change, can influence the solubility of gases, the metabolic rate of aquatic flora and fauna, the evaporation rate of open waters and the formation of ice. Besides, water temperature changes have effects not only locally, but also regionally and downstream (OLDEN & NAIMAN 2010). For example, more water is needed to cool power plants, as the higher temperature results in lower cooling potential (VAN VLIET ET AL. 2016). In addition, higher water temperatures can increase the evaporation rate and hence lead to lower water availability (WANDERS & WADA 2015). Also, fish and other aquatic flora and fauna may die (MATTHEWS & BERG 1997) if less oxygen can be dissolved in the water due to the higher temperatures (OZAKI ET AL. 2003). This also promotes the proliferation of cyanobacteria (ROBARTS & ZOHARY 1987). Water temperature is also relevant to the formation of ice. Since flooding can occur due to ice accumulation (WANDERS ET AL. 2019), it is necessary to obtain data for the forecast.

To quantify the heat uptake by inland waters, which is an essential topic for understanding the response of the earth system to greenhouse gas emissions, as, e.g., done by VANDERKELEN ET AL. (2020), the water temperatures and the corresponding volumes are needed. Unfortunately, these values, as observations, are sparse and spatially limited. Hence, in order to assess the effects of changes in water temperature, a good spatial and temporal resolution of water temperatures on a global scale is required. Especially in areas that cannot be observed, modeling is the only way to approximate water temperatures over long periods (WANDERS ET AL. 2019). VANDERKELEN ET AL. (2020) had to use several different models to obtain water volumes and temperatures. One model (SIMSTRAT-UoG by GOUDSMIT ET AL. (2002)) for calculating water volumes could not represent human influences, which is a significant factor. To determine the water temperature, the global nonlinear regression model of PUNZET ET AL. (2012) was used. A global water use and water availability model like WaterGAP, which can also calculate the water temperature, especially for the different compartments such as rivers, lakes and reservoirs separately, would help for further research on this topic and everything mentioned above.

Therefore, the subject of this master thesis is to implement the water temperature computation according to VAN BEEK ET AL. (2012) and WANDERS ET AL. (2019) into WaterGAP, evaluate the results and simulate the water temperature changes due to climate change until 2099. Also, these results are compared to the regression model of PUNZET ET AL. (2012) to evaluate the regression model's performance in scenarios of the future with changing environmental parameters.

Essentially, two types of approaches are used to model water temperature: statistical and physical (CAISSIE 2006). A statistical approach calculates the water temperature, e.g., by utilizing regression (e.g., PUNZET ET AL. (2012)). Statistical methods are based on existing observations and usually achieve satisfactory results provided that the environmental parameters do not change. Otherwise, extrapolation is difficult (CAISSIE 2006). Moreover, they are hardly ever applied on a global scale (PUNZET ET AL. 2012). In contrast, physical models use the links

between water temperature and hydrological and meteorological variables to calculate the energy exchange between water and atmosphere (VAN BEEK ET AL. 2012; WANDERS ET AL. 2019). However, compared to statistical approaches, this requires more data and more computing capacity (e.g., CAISSIE (2006)). These models are already used for historical (VAN BEEK ET AL. 2012) and future global calculations of water temperature (VAN VLIET ET AL. 2013). Another physical approach is the solution of 1D heat advection using a semi-lagrange approach (YEARSLEY 2009). This has already been used to calculate the change of the water cooling potential during climatic changes (VAN VLIET ET AL. 2016). With the help of physical models, predictions can be made about the effects of climate change and about areas that are difficult to monitor on a global scale (WANDERS ET AL. 2019).

In this thesis, the approach of YEARSLEY (2009) is not further pursued, since it only includes the balance of radiation energy and the advected heat by inflows. In contrast, the approach of VAN BEEK ET AL. (2012) already considers more physical processes. WANDERS ET AL. (2019) is based on VAN BEEK ET AL. (2012) with several changes, some of which VAN BEEK ET AL. (2012) already proposed. These are the consideration of mechanical ice breakup by assuming a minimum ice cover of 5 mm, transportation of the broken ice in the river and considering the thermocline in lakes and reservoirs. When a thermocline is formed, the water volume interacting with the atmosphere is reduced to the water above the thermocline. The resolution used by WANDERS ET AL. (2019) was increased from 50 km to 10 km at the equator, which is very difficult to implement in WaterGAP. However, the implementation of the water temperature in WaterGAP is still feasible because the average monthly water temperature is a required output since the ISIMIP2a protocol. After the implementation of the water temperature, WaterGAP will again reflect the current state of research. Furthermore, the water temperature is of great importance for the biodiversity and water quality sectors, so it is crucial that several models can compute and output this temperature.

1.1.1. Calculation of the Water Temperature According to PUNZET ET AL. (2012)

PUNZET ET AL. (2012) assume a non-linear relationship between water and air temperature for their regression approach. This function resembles an s-shaped curve. To determine the coefficients of the non-linear regression model, they use data from the USGS (U.S. Geological Survey) and the UNEP-GEMS (United Nations Environmental Program - Global Environment Monitoring System) as well as from various water level gauging stations across Europe. As a mathematical representation of this s-shaped curve PUNZET ET AL. (2012) used equation 1.1.

$$T_{Water} = \frac{C_0}{1 + e^{(C_1 \cdot T_{Air} + C_2)}} \quad (1.1)$$

where

- T_{Water} = water temperature [°C]

- T_{Air} = air temperature [$^{\circ}\text{C}$]
- C_0 = upper bound water temperature [$^{\circ}\text{C}$]
- C_1 = steepest slope of the function [$^{\circ}\text{C}^{-1}$]
- C_2 = measure for inflexion point of the function [$^{\circ}\text{C}$] (inflexion point = $-C_2/C_1$)

Table 1.1 shows the regression parameters calculated by PUNZET ET AL. (2012) for the five different climate zones and their respective fitting coefficients.

Table 1.1.: The results of the curve fitting by PUNZET ET AL. (2012) showing the three fitting coefficients and respective efficiencies: quality of fit for calibrated (calib) and validated (valid) datasets.

| | C_0 | C_1 | C_2 | NSC | | RMSE | |
|----------------|-------|-------|-------|-------|-------|-------|-------|
| | | | | Calib | Valid | Calib | Valid |
| Warm temperate | 32 | -0.13 | 1.94 | 0.82 | 0.83 | 2.9 | 2.6 |
| Snow | 32 | -0.14 | 2.08 | 0.84 | 0.88 | 3.1 | 2.4 |
| Arid | 32 | -0.12 | 1.82 | 0.81 | 0.88 | 3.6 | 2.7 |
| Equatorial | 32 | 0.18 | 3.02 | 0.22 | 0.20 | 3.3 | 2.9 |
| Polar | 32 | -0.11 | 2.15 | 0.66 | 0.56 | 1.8 | 2.0 |
| Global | 32 | -0.13 | 1.94 | 0.88 | 0.88 | 3.0 | 2.6 |

1.1.2. Calculation of the Water Temperature According to VAN BEEK ET AL. (2012)

TOPRAK & SAVCI (2007) modeled the dispersion coefficients in natural river courses. For the average values, advection already becomes the dominant factor at a channel length of 100 m, a flow velocity of 1 ms^{-1} and a temperature difference of 1°C , which is why the dispersion term is usually neglected in studies of natural river systems (YEARSLEY 2009). In VAN BEEK ET AL. (2012), lateral heat transport also occurs only via advection. Here the energy balance of water with constant density is modeled, which flows through a rectangular channel with perfect vertical and lateral mixing (see fig. 1.1). Therefore daily timesteps and a grid with a spatial resolution of 0.5° are used as an Eulerian reference system (VAN BEEK ET AL. 2012). Equation 1.2 is used for the energy balance of surface water [$\text{J m}^{-2} \text{ s}^{-1}$] per unit width w [m].

$$\rho_w C_p \frac{\partial (h T)}{\partial t} = -\rho_w C_p \frac{\partial (v h T)}{\partial x} + S^{\downarrow} (1 - \alpha) + L^{\downarrow} - L^{\uparrow} - H - \lambda \rho_w E + \rho_w C_p \sum_{i=1}^M q_{s,i} T_{s,i} \quad (1.2)$$

with

- ρ_w = density of water [kg m^{-3}]

- C_p = heat capacity of water [$\text{J kg}^{-1} \text{K}^{-1}$]
- h = water height [m]
- T = water temperature [K]
- t = time [T]
- v = average flow velocity [m s^{-2}]
- x = location in drainage network [L]
- S^\downarrow = incoming shortwave radiation [$\text{J s}^{-1} \text{m}^{-2}$]
- α = albedo of water or ice
- L^\downarrow = incoming longwave radiation [$\text{J s}^{-1} \text{m}^{-2}$]
- L^\uparrow = outgoing longwave radiation [$\text{J s}^{-1} \text{m}^{-2}$]
- H = sensible heat flux [$\text{J s}^{-1} \text{m}^{-2}$]
- $\lambda \rho_w E$ = latent heat flux due to evaporation [$\text{J s}^{-1} \text{m}^{-2}$] with
 - λ = latent heat of vaporization [$\text{J s}^{-1} \text{m}^{-2}$]
 - E = open water evaporation [m s^{-1}]
- $\rho_w C_p \sum_{i=1}^M q_{s,i} T_{s,i}$ = sum of inflowing water fluxes

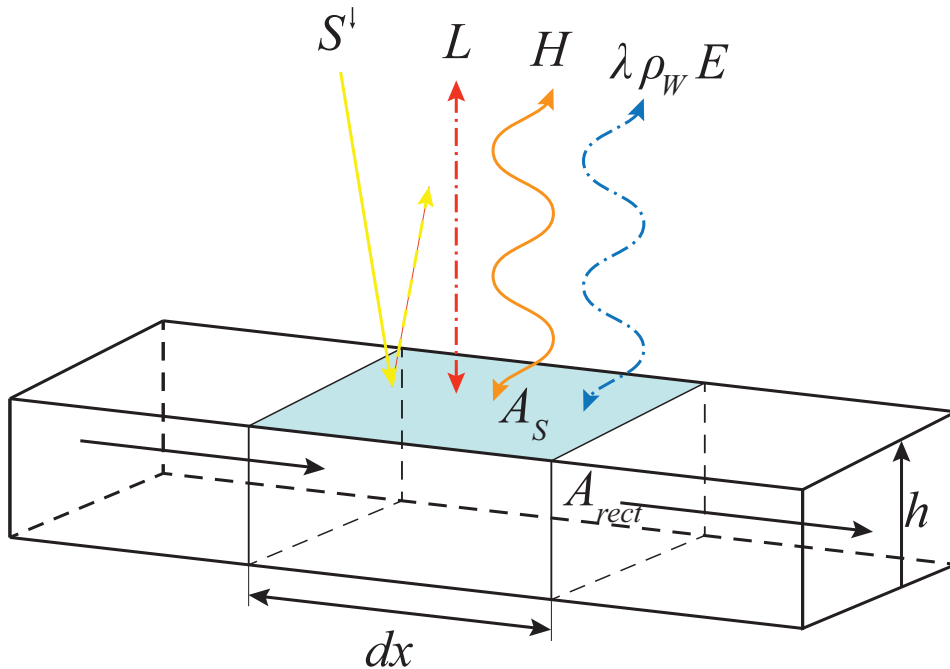


Figure 1.1.: A schematic representation of the energy balance in a rectangular channel according to VAN BEEK ET AL. (2012) with A_s the surface area, A_{rect} the cross-sectional area of the channel and the depth h . (image like VAN BEEK ET AL. (2012))

The sensible heat flux between water and atmosphere is calculated with equation 1.3. T_{atmo} is the air temperature [K] 2 m above ground.

$$H = K_H(T - T_{atmo}) \quad (1.3)$$

The sum as the last term on the right side of equation 1.2 includes, e.g., precipitation, surface runoff, as well as the base flow with their quantities [$\text{m}^3 \text{s}^{-1}$] and their temperatures [K]. In this sum, other anthropogenic effects, such as cooling water from power plants, can also be taken into account. VAN BEEK ET AL. (2012) calculates the energy balance as follows. First, the vertical changes in the energy balance per cell and then the lateral transport along the drainage network are considered. The derivative over time in the vertical energy balance is calculated using the forward difference method. The lateral transport, which is computed by the global hydrological Model PCR-GLOBWB, includes a local and temporal derivative. This derivative is calculated using the backward difference method (VAN BEEK ET AL. 2012).

The formation of ice is taken into account by adjusting the albedo. Ice forms as soon as the air temperature falls below 0°C and the sensible heat flux and the incoming radiation are not sufficient to keep the water temperature above 0°C . The thickness of the ice increases with continuous cooling until the current cell under consideration is completely frozen. The resulting ice can not cool below 0°C and influences the roughness of the cell's drainage network, which in turn has an influence on the flow rate (VAN BEEK ET AL. 2012). If ice is present, the latent heat flux is assumed zero and two sensible heat fluxes are considered. One is between water and ice, the other between ice and atmosphere (equations 1.4 and 1.5) with the turbulent heat exchange coefficient K_H [$\text{Js}^{-1} \text{m}^{-2} \text{K}^{-1}$] (VAN BEEK ET AL. 2012). The ice thickness and its changes are computed with equation 1.6 with λ_f [kJkg^{-1}] as the latent heat of fusion of ice.

$$H_1 = K_H(T - 273) \quad (1.4)$$

$$H_2 = K_H(273 - T_{atmo}) \quad (1.5)$$

$$\lambda_f \rho_w \frac{dz}{dt} = -H_1 + H_2 - S^\downarrow(1 - \alpha) - L^\downarrow + L^\uparrow \quad (1.6)$$

2. Methodological Approach

2.1. Implementation of the Water Temperature in WaterGAP

The computation of the water temperature is implemented into WaterGAP according to VAN BEEK ET AL. (2012) and WANDERS ET AL. (2019). WaterGAP is programmed in C++ and Clion by JetBrains is used as a development environment. Several different R-scripts for the evaluation, validation, as well as the analysis of scenarios, are created with RStudio (RSTUDIO TEAM 2020) (see appendix A.1.3). The calculated water temperatures [°C] can be saved in four different ways:

- daily values
- monthly mean values
- separately for all surface water bodies (see fig. 2.1) as daily values
- separately for all surface water bodies (see fig. 2.1) as monthly mean values

-9999 in the output data indicates that no water temperature could be calculated at this point in time because, e.g., there is no such surface water body present in the cell or no water volume was present. Figures 2.1 and 2.2 show the routing of water in WaterGAP and the corresponding water temperature calculation. The groundwater and the surface runoff flow into the first surface water body existing in the cell. The water flows through every existing surface water body in the cell in one time step in the order seen in figure 2.1.

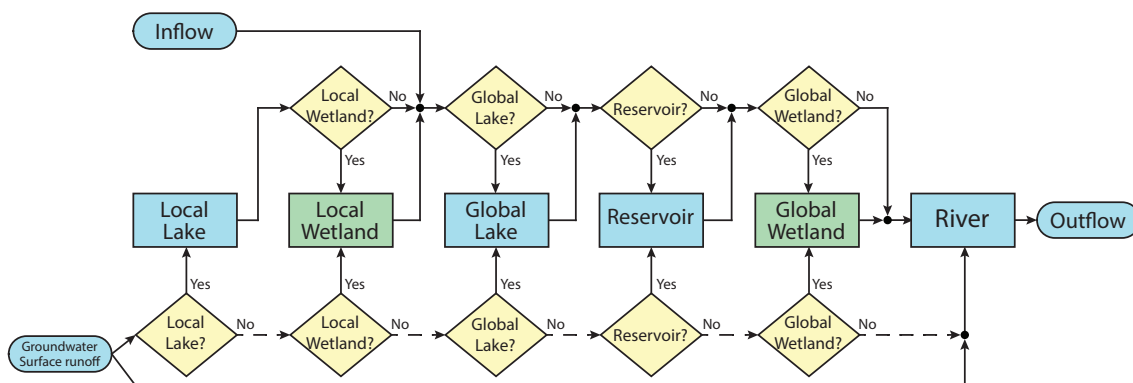
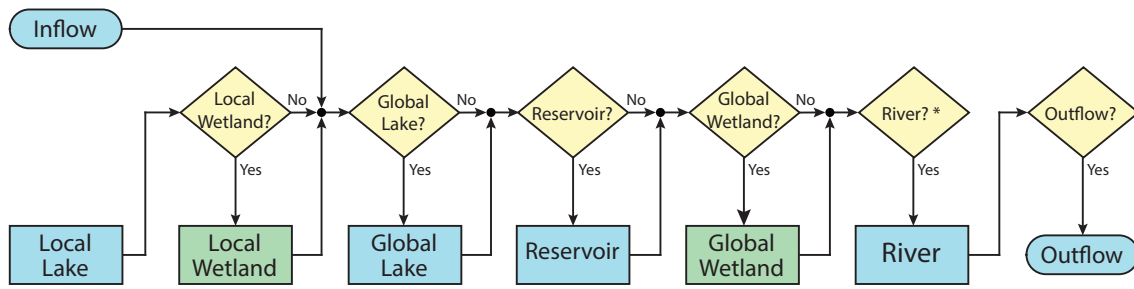


Figure 2.1.: The flow of the water in WaterGAP. A local lake flows into local wetlands if their area is greater than zero in the current cell. Then the water flow merges with the inflow from the cell upstream etc.



* River is present, if river length in WaterGAP unequal 55 km or cell has outflow

Figure 2.2.: The corresponding water temperature calculation to the flow of the water in WaterGAP. In some cells, the river is not calculated if its length is 55 km (default initialization value in WaterGAP) and the current cell has no cell downstream.

Several assumptions have to be made. The water temperature cannot drop below 0 °C and cannot exceed 60 °C. If the water temperature is greater than 60 °C, it will reset to the current air temperature to eliminate instabilities in the model due to small water volumes. 60 °C is chosen because the highest ever measured air temperature worldwide is 56.7 °C (FADLI ET AL. 2013). How this assumption influences the results of scenarios of the future under climate change conditions has to be pondered.

The initialization value for the water temperature at the start of a WaterGAP model run is set to 15 °C, which is consistent with a standard atmosphere defined by the ICAO (International Civil Aviation Organization), which describes a mean state of the atmosphere and its properties like pressure, temperature and density (ICAO 1993). This assumption is insignificant because if WaterGAP is started with default settings, the first year is run five times as an initialization phase before output data is created. After the first initialization year, the water temperature is already close to the air temperature and little to no changes happen over the remaining four initialization years.

Other assumptions are the groundwater temperature is assumed as the mean air temperature over each year, as in VAN BEEK ET AL. (2012) but cannot be below 0 °C. Furthermore, the precipitation temperature is assumed as the maximum of the air temperature minus 1.5 °C and 0 °C. The air temperature is lowered by 1.5 °C to simulate colder precipitation because it originates in higher altitudes, also like it is done in VAN BEEK ET AL. (2012). The surface runoff temperature equals the precipitation temperature.

If the water volume of a surface water body reaches zero, no water temperature calculation can be made. It is then reset to the current air temperature to ensure calculation safety since a temperature from the previous time step is always needed. This temperature should never be used by the program because there is no corresponding water volume, but it might happen due to calculation inaccuracies.

An additional logic is implemented for the sensible heat flux so that the water can only be heated or cooled to the air temperature due to the sensible heat flux. This is done to counter instabilities in the model if the air temperature experiences large jumps from one timestep to the next.

The depth of the thermocline is only computed in global lakes and reservoirs with equation 2.1 (WANDERS ET AL. 2019). It is not reasonable to calculate the thermocline in local lakes because all small lakes of one cell are aggregated together and thus do not depict a real lake.

$$D_t = 9.52 \cdot f^{0.425} \quad (2.1)$$

f in equation 2.1 represents the so-called fetch-length, which is the longest possible length, depending on the predominant wind direction, the wind can blow over the water surface unhindered. Gathering the predominant wind direction and geometry of every global lake and reservoir is impossible. After consulting Dr. Wanders via e-mail, on how they calculated the fetch-length in WANDERS ET AL. (2019), it is implemented in WaterGAP as follows. Global lakes are assumed as squares and their fetch-length is the diagonal. Reservoirs are approximated as equilateral triangles with the height of the triangle as their fetch-length.

The water volume which evaporates from rivers and the surface area of the rivers are not calculated in WaterGAP as of May 2020. There are still unsolved problems with the surface area calculation of rivers and the reduction of said area due to the evaporation. In the water temperature calculation, however, the evaporation from rivers is calculated because it is a main energy sink to cool the rivers. This leads to small inconsistencies in the water volume of rivers between the water volume calculation and the temperature calculation of said water. The evaporation volume is calculated under the assumption of a trapezoidal cross-sectional area of the riverbed (see fig. 2.3). This leads to a river surface area under consideration of the river length and the water volume stored in the river.

The impacts of the inflow from water use, e.g., irrigation, cannot be taken into account because no suitable temperature can be assumed. This is due to the fact that every use is aggregated for the volume calculation, but every use produces different water temperatures. The only exception is the water use for cooling power plants. It is assumed that the water is discharged back into the river with an additional 3 °C compared to the river temperature. There is no data available if this is a correct assumption, but the results for the river Rhine, which is heavily influenced by power plant cooling, and other rivers are promising (see chapter 3).

If the water temperature reaches 0 °C, ice might form as in VAN BEEK ET AL. (2012), but there is no influence on the river channel's roughness. To simulate mechanical ice breakup, a minimum ice thickness of 5 mm is required in the river due to the flowing water (WANDERS ET AL. 2019). The maximum ice thickness for every surface water body is reached if the ice volume equals the stored water volume. The ice thickness is calculated if there already was ice in the previous time step, or the air temperature is below 0 °C. After that, if the ice thickness is not at its maximum, the water temperature of the remaining water below the ice is calculated.

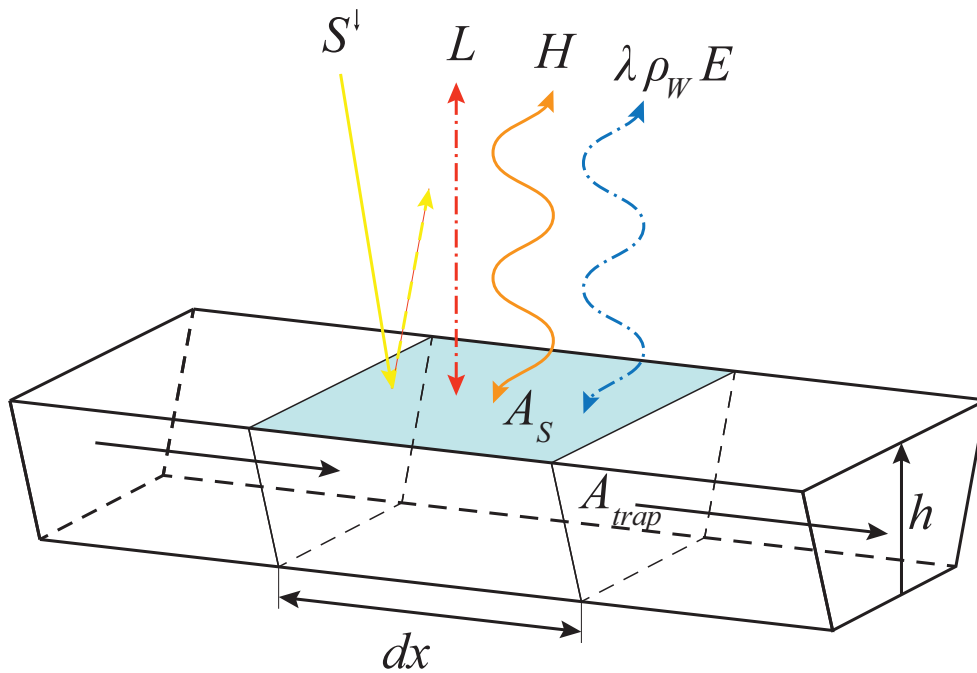


Figure 2.3.: A schematic representation of the energy balance in a trapezoidal channel of WaterGAP with A_S the surface area, A_{trap} the cross-sectional area of the channel and the depth h . (image like VAN BEEK ET AL. (2012))

To counter computational problems resulting from very small water volumes in rivers, especially in cells that reflect small islands, a query is implemented to check if the river length equals 55 km and if the cell has no downstream cell. If the two queries return true, the calculation of the river is omitted and the output water temperature is the temperature of the last existing surface water body (see fig. 2.2) in the cell. 55 km is the initialization value for the river length in WaterGAP, which is typically altered by a meandering ratio to accommodate the river's meandering. The query returns true for 1064 cells of the total 67420 cells, equaling about 1.6%. These cells are mostly the coastal cells of Greenland and the before mentioned small islands in the Pacific and the Atlantic Ocean (see fig. 2.4). In reality, small islands do not have rivers that long or with significant amounts of water volume. The mentioned query thus enables WaterGAP to calculate the water temperature more realistically for these islands. This also leads to no data entries (-9999) for some islands because the river was the only surface water body present in the model and now no water temperature is calculated.



Figure 2.4.: The red cells indicate where a river calculation is omitted.

For equations 1.2 to 1.6 several constants are required:

- $\rho_w = 1000 \text{ kg m}^{-3}$
- $C_p = 4180 \text{ J kg}^{-1} \text{ K}^{-1}$
- $\alpha_{water} = 0.08$ (WaterGAP)
- $\alpha_{ice} = 0.6$ (WaterGAP)
- $K_H = 20 \text{ J s}^{-1} \text{ m}^{-2} \text{ K}^{-1}$ ice/water to atmosphere (eq. 1.3 and 1.5); (VAN BEEK ET AL. 2012)
- $K_H = 8 \text{ J s}^{-1} \text{ m}^{-2} \text{ K}^{-1}$ water to ice (eq. 1.4); (VAN BEEK ET AL. 2012)
- $\lambda_f = 333.4 \text{ kJ kg}^{-1}$ (VAN BEEK ET AL. 2012)

The outgoing longwave radiation L^\uparrow is calculated with the Stephan-Boltzmann equation (see equation 2.2) with the emissivity $\varepsilon = 1$ and the Stephan-Boltzmann constant $\sigma = 5.670 \cdot 10^{-8} \text{ W m}^{-2} \text{ K}^{-4}$.

$$L^\uparrow = \varepsilon \cdot \sigma \cdot T^4 \quad (2.2)$$

The latent heat of vaporization in equation 1.2 depends on the air temperature and can be calculated with equation 2.3, which was already implemented in WaterGAP. It is assumed zero, if an ice cover is present.

$$\lambda = 2.501 - 0.002361 \cdot T_{atmo} \cdot 10^6 \text{ [J]} \quad (2.3)$$

For the coefficients, C_0 , C_1 and C_2 of equation 1.1, used for comparison of the results of the WaterGAP implementation with the approach of PUNZET ET AL. (2012), the global results of the curve fitting from PUNZET ET AL. (2012) are chosen (see table 1.1).

- $C_0 = 32$
- $C_1 = -0.13$
- $C_2 = 1.94$

2.2. Climate Forcing Data Used for WaterGAP Runs

The WFDEI meteorological forcing data set (WATCH Forcing Data methodology applied to ERA-Interim reanalysis data) (WEEDON ET AL. 2014) was used for validation. It is an improvement over the WATCH Forcing Data (WFD) by utilizing the ERA-Interim reanalysis data to gain better results, e.g., for precipitation, wind speed and downward shortwave fluxes (WEEDON ET AL. 2014). For the simulation of the future under climate change conditions, the climate forcing IPSL-CM5A-LR (PIK n.d.) with its four scenarios RCP2.6, RCP4.5, RCP6 and RCP8.5 was used.

2.3. Data and Coefficients Used for Validation of Model Results

2.3.1. Observed Data

To conduct the validation, real world measured water temperature data is gathered from the Global Freshwater Quality Database data portal, which is a part of the GEMS/Water Program of the United Nations Environment Program (UNEP) (ICWRGC n.d.). Attention is paid to ensure that the data is obtained without significant gaps of several years and that several values per year are available. Efforts also are made to reflect different climate zones with the choice of the rivers. This screening, combined with checking the representation of the river in WaterGAP, lead to a selection of 62 stations globally for validation (see fig. 2.5 and table 2.1). Africa is only represented by one station because the quality and the availability of data are lacking. Furthermore, the river Rhine is chosen with 8 out of the 62 stations to investigate the water temperature calculation with an expanding catchment area. The Rhine data availability is very good, with very few data gaps over a long time frame. Also, two of the chosen stations (DEU00006 and NLD00001) are within one grid cell of WaterGAP, without another river flowing into the Rhine in between these two stations in real life (see fig. 3.3). Therefore those two stations are beneficial to demonstrate the impact of data availability on the validation.



Figure 2.5.: All the globally selected measuring stations of the Global Freshwater Quality Database. (ICWRGC n.d.)

Table 2.1.: All 62 stations taken from the Global Freshwater Quality Database (ICWRGC n.d.) from which measured water temperature data is used for validation with the coordinates, the river and the country they are located. The three letters at the beginning of the station name indicate the country according to ISO-3166 Alpha-3.

| Station | Lon | Lat | River |
|---------------------------|--------------|--------------|------------------|
| Africa | | | |
| SDN00002 | 15.5 | 32.46333333 | Blue Nile River |
| Asia & Oceania | | | |
| AUS00004 | -34.06666667 | 141.2416667 | Murray River |
| AUS00005 | -34.91722222 | 139.3083333 | Murray River |
| CHN00001 | 30.58305556 | 114.8288889 | Yangtze River |
| CHN00002 | 36.73333333 | 116.9833333 | Yellow River |
| CHN00007 | 37.5 | 118.2333333 | Yellow River |
| CHN00008 | 32 | 120.85 | Yangtze River |
| IND00007 | 21.91666667 | 73.65 | Narmada River |
| IND00031 | 10.94277778 | 78.44138889 | Cauvery River |
| IND00047 | 21.28361111 | 72.95 | Tapti River |
| JPN00003 | 36.18055556 | 139.475 | Tone River |
| KHM00003 | 12 | 105.4666667 | Mekong River |
| KHM00006 | 12.47 | 106.0158333 | Mekong River |
| NZL00014 | -37.43209689 | 175.131536 | Waikato |
| NZL00071 | -45.66474969 | 169.4100638 | Clutha |
| NZL00075 | -46.23727757 | 169.7479876 | Clutha |
| PAK00006 | 25.23 | 68.31166667 | Indus River |
| THA00002 | 15.67083333 | 100.1125 | Chao Phrya River |
| THA00015 | 16.35 | 102.9633333 | Nam Chi River |
| Europe | | | |
| CHE00001 | 47.38444444 | 9.642222222 | Rhine River |
| CHE00002 | 47.57055556 | 8.330833333 | Rhine River |
| CHE00003 | 47.56667 | 7.585 | Rhine River |
| DEU00001 | 49.03333333 | 8.302777778 | Rhine River |
| DEU00002 | 50 | 8.23 | Rhine River |
| DEU00003 | 50.25 | 7.647777778 | Rhine River |
| DEU00006 | 51.83972222 | 6.17 | Rhine River |
| ESP00008 | 41.48 | -4.97 | Douro River |
| ESP00011 | 40.04138889 | -3.6 | Tejo River |
| ESP00012 | 39.95 | -4.82 | Tejo River |
| ESP00013 | 39.72 | -6.895833333 | Tajo River |
| FRA00006 | 47.88333333 | 1.916666667 | Loire River |

continued on next page

| Station | Lon | Lat | River |
|----------------------|--------------|--------------|-----------------------|
| FRA00007 | 47.40333333 | -0.915833333 | Loire River |
| FRA00015 | 45.18333333 | 4.816666667 | Rhone River |
| GBR00001 | 51.42888889 | -0.317222222 | Thames River |
| GBR00004 | 52.93861111 | -1.135 | Trent River |
| HUN00002 | 47.61 | 19.09666667 | Danube River |
| NLD00001 | 51.85 | 6.101666667 | Rhine River |
| POL00006 | 53.035 | 14.31277778 | Odra River |
| PRT00001 | 39.22638889 | -8.676111111 | Tejo River |
| North America | | | |
| CAN00005 | 59.86944444 | -111.5861111 | Slave River |
| CAN00006 | 49.09166667 | -96.69166667 | Roseau River |
| CAN00007 | 49.3875 | -121.45 | Fraser River |
| CAN00052 | 45.16972 | -67.29722 | St. Croix River |
| USA00007 | 38.92944444 | -77.11722222 | Potomac River |
| USA00011 | 38.45555556 | -121.5019444 | Sacramento River |
| USA00012 | 34.66861111 | -92.155 | Arkansas River |
| Russia | | | |
| RUS00004 | 56.56861111 | 84.9 | Tom River |
| RUS00005 | 55.20277778 | 73.20555556 | Irtys River |
| RUS00008 | 46.75555556 | 47.81388889 | Volga River |
| RUS00011 | 66.61944444 | 66.55 | Ob River |
| RUS00012 | 67.58333333 | 52.17527778 | Pechora River |
| RUS00015 | 47.53416667 | 40.6475 | Don River |
| RUS00018 | 70.66666667 | 127.3333333 | Lena River |
| RUS00028 | 72.33333333 | 126.6666667 | Lena River |
| RUS00043 | 64.14305556 | 41.92222222 | Severnaya Dvina River |
| South America | | | |
| ARG00005 | -34.31555556 | -58.50111111 | Plata River |
| ARG00012 | -27.43333333 | -57.33333333 | Parana River |
| BRA00018 | -3.3105556 | -60.609444 | Solimoes River |
| BRA00086 | -24.066667 | -54.25 | Parana River |
| BRA00123 | -1.9469444 | -55.5108333 | Amazonas River |
| BRA02104 | -21.296944 | -49.795 | Rio Tietê |
| BRA02112 | -22.6611 | -51.3883 | Rio Paranapanema |

2.3.2. Coefficients

To validate the model, three coefficients are chosen: the Nash-Sutcliffe Efficiency (NSE, eq. 2.4), the Root-Mean-Square Error (RMSE, eq. 2.5) and the Kling-Gupta Efficiency (KGE (year 2012 method), eq. 2.6). All three coefficients are computed with the hydroGOF package (ZAMBRANO-BIGIARINI 2020) for R. The NSE is a normalized statistic that determines the relative magnitude of the residual variance ("noise") compared to the measured data variance ("information") (NASH & SUTCLIFFE 1970). It ranges from $-\infty$ to 1. The closer it is to 1, the more accurate the model is with a perfect match if $NSE = 1$. If the NSE is ≤ 0 , the mean of the observed data predicts values as good as or better than the model. The RMSE indicates the standard deviation of the model prediction error. The smaller the value, the better the model performance. The KGE developed by GUPTA ET AL. (2009) is a measure for the goodness of fit. It helps to analyze the relative importance of the different components of the NSE. Three components are calculated: the Pearson product-moment correlation r , the ratio between the coefficient of variation of the simulated and observed values γ and the ratio between the mean of the simulated and the observed values β . All three have an ideal value of 1. Like the NSE, the KGE ranges from $-\infty$ to 1. The closer to 1, the more accurate the model is. S and O in equations 2.4, 2.5 and 2.6 stand for simulated and observed values. \bar{O} in equation 2.4 is the mean value of the observed data.

$$NSE = 1 - \frac{\sum_{i=1}^N (S_i - O_i)^2}{\sum_{i=1}^N (O_i - \bar{O})^2} \quad (2.4)$$

$$RMSE = \sqrt{\text{mean}((S - O)^2)} \quad (2.5)$$

$$KGE = 1 - \sqrt{(r - 1)^2 + (\gamma - 1)^2 + (\beta - 1)^2} \quad (2.6)$$

$$\gamma = \frac{CV_S}{CV_O}; \quad \beta = \frac{\mu_S}{\mu_O}$$

A sensitivity analysis is conducted regarding the input values of the groundwater temperature, the temperature increase of the discharged water used for cooling power plants and the decrease of the precipitation and surface runoff temperature to estimate the influence of the assumptions made regarding these three input values. The sensitivity S is calculated with equation 2.7, with result R and parameter P .

$$S = \frac{\frac{dR}{R}}{\frac{dP}{P}} \quad \text{with} \quad \frac{dR}{R} = \frac{(R_2 - R_1)}{R_1} \quad \text{and} \quad \frac{dP}{P} = \frac{(P_2 - P_1)}{P_1} \quad (2.7)$$

3. Evaluation and Validation

3.1. Model Variations

For the validation of the model, several different model variations are computed between 1965 and 2016. This is achieved by activating or deactivating various WaterGAP options before every run or changing of variables in the code (see table 3.1). The standard run is calculated with activated reservoirs and human water use, as well as power plant cooling, which increases the temperature of the used water by 3 °C. Also, ice formation in surface water bodies is possible. The groundwater temperature is equal to the yearly mean air temperature of the specific cell. Relative to the air temperature, the precipitation and, hence, the surface runoff are cooled by 1.5 °C.

In two other simulations, the power plant cooling water temperature is increased by 5 and 10 °C. A third simulation discharges the used water back into the river with a temperature of 30 °C and a fourth run is done without considering power plant cooling. A completely natural run is computed without power plant cooling, reservoirs and human use. One run is simulated without human use another without reservoirs. Once the cooling of the precipitation and surface runoff by 1.5 °C is omitted and once no ice can form on the surface water bodies. Finally, the groundwater temperature influence is evaluated by setting the groundwater temperature to a constant 4 °C and 10 °C as well as the yearly mean air temperature with a maximum of 25 °C. The maximum of 25 °C is chosen after looking at groundwater temperature data near the equator in the Global Freshwater Quality Database.

For the simulation of the future water temperatures under climate change conditions, the time period is from 1861 to 2099. The four scenarios RCP2.6, RCP4.5, RCP6 and RCP8.5 of the IPSL-CM5A-LR (PIK n.d.) climate forcing are computed. They all are simulated without human use and power plant cooling for a better comparison with PUNZET ET AL. (2012) because these anthropogenic effects are not taken into account in this approach.

Table 3.1.: An overview of the computed scenarios for validation and their differences compared to the standard run (✓ means like standard run).

| Scenario | Variables | | | | | |
|--------------------|------------------------------------|-----------|--|-----------|-----------------|-----|
| | Groundwater | Reservoir | Power plants | Water use | Precip. cooling | Ice |
| Standard run | yearly mean air temperature (ymat) | yes | river t. +3 °C | yes | air t. -1.5 °C | yes |
| Groundwater | 4 °C, 10 °C, ymat max. 25 °C | ✓ | ✓ | ✓ | ✓ | ✓ |
| Power plants | ✓ | ✓ | no power plants, river t. +5 °C, river t. +10 °C, 30 °C | ✓ | ✓ | ✓ |
| No ice | ✓ | ✓ | ✓ | ✓ | ✓ | — |
| No water use | ✓ | ✓ | ✓ | — | ✓ | ✓ |
| No precip. cooling | ✓ | ✓ | ✓ | ✓ | — | ✓ |
| Natural run | ✓ | — | — | — | ✓ | ✓ |
| No reservoir | ✓ | — | ✓ | ✓ | ✓ | ✓ |

3.2. Standard Simulation Run

Table 3.2 shows the results for NSE, KGE and RMSE of the standard simulation run and for computed regression model results according to PUNZET ET AL. (2012). The median and average values of the NSE, KGE and RMSE for the simulation with WaterGAP and the regression model by PUNZET ET AL. (2012) can be seen in table 3.3. Figures 3.1 and 3.2 show boxplots of the KGE, r , β and γ for the whole world and for five of the six geographic zones mentioned earlier. Africa has only one station, so a boxplot is not feasible. The average worldwide NSE and RMSE (table 3.3) for WaterGAP are distorted by station AUS00004, where WaterGAP failed to produce a reasonable result. Without AUS00004, the averages would be 0.21 (NSE) and 3.42 (RMSE). The KGE of the WaterGAP model and the regression model are relatively close, but the regression model yields better results overall. Also, r , β and γ are very similar and close to their optimal value of 1. Asia & Oceania, as well as South America, show poor results for the average NSE. Europe and Russia show excellent results.

Table 3.2.: All results for NSE, KGE, and RMSE of every station of the standard simulation run for comparison with the regression model of PUNZET ET AL. (2012).

| Station | WaterGAP | | | | | | Regression Model | | | | | |
|---------------------------|----------|------|------|---------|----------|-------|------------------|------|------|---------|----------|------|
| | NSE | KGE | r | β | γ | RMSE | NSE | KGE | r | β | γ | RMSE |
| Africa | | | | | | | | | | | | |
| SDN00002 | -2.00 | 0.55 | 0.68 | 1.26 | 0.83 | 7.83 | 0.28 | 0.35 | 0.63 | 1.05 | 0.47 | 3.83 |
| Asia & Oceania | | | | | | | | | | | | |
| AUS00004 | -12.61 | 0.05 | 0.82 | 1.81 | 1.46 | 16.86 | 0.93 | 0.92 | 0.97 | 1.01 | 1.08 | 1.22 |
| AUS00005 | -0.61 | 0.54 | 0.97 | 1.23 | 1.39 | 5.14 | 0.90 | 0.85 | 0.98 | 0.95 | 1.14 | 1.28 |
| CHN00001 | 0.80 | 0.81 | 0.97 | 1.09 | 1.17 | 3.18 | 0.90 | 0.88 | 0.96 | 0.98 | 1.11 | 2.22 |
| CHN00002 | 0.89 | 0.81 | 0.97 | 1.16 | 0.91 | 3.22 | 0.90 | 0.75 | 0.97 | 1.12 | 0.79 | 3.05 |

continued on next page

| Station | WaterGAP | | | | | | Regression Model | | | | | |
|----------------------|----------|------|------|---------|----------|------|------------------|-------|------|---------|----------|------|
| | NSE | KGE | r | β | γ | RMSE | NSE | KGE | r | β | γ | RMSE |
| CHN00007 | 0.82 | 0.80 | 0.95 | 1.17 | 0.91 | 3.95 | 0.86 | 0.79 | 0.94 | 1.12 | 0.83 | 3.55 |
| CHN00008 | 0.88 | 0.90 | 0.97 | 1.08 | 1.06 | 2.72 | 0.89 | 0.92 | 0.95 | 0.95 | 1.02 | 2.62 |
| IND00007 | -1.05 | 0.47 | 0.51 | 1.11 | 1.17 | 4.95 | 0.28 | 0.46 | 0.56 | 0.98 | 0.69 | 2.94 |
| IND00031 | -0.37 | 0.14 | 0.21 | 1.07 | 0.67 | 6.31 | -0.21 | -0.17 | 0.16 | 0.91 | 0.19 | 5.95 |
| IND00047 | -2.30 | 0.40 | 0.44 | 1.13 | 1.19 | 5.18 | 0.26 | 0.40 | 0.55 | 0.98 | 0.6 | 2.45 |
| JPN00003 | 0.84 | 0.79 | 0.95 | 1.00 | 1.20 | 2.66 | 0.89 | 0.91 | 0.97 | 1.06 | 1.06 | 2.18 |
| KHM00003 | -0.38 | 0.70 | 0.74 | 1.06 | 0.86 | 2.08 | -1.16 | 0.30 | 0.71 | 0.93 | 0.37 | 2.60 |
| KHM00006 | -0.88 | 0.28 | 0.30 | 1.05 | 0.88 | 2.65 | -1.04 | 0.17 | 0.45 | 0.93 | 0.38 | 2.76 |
| NZL00014 | 0.74 | 0.64 | 0.95 | 1.01 | 1.35 | 1.95 | 0.81 | 0.91 | 0.97 | 0.92 | 0.97 | 1.69 |
| NZL00071 | 0.33 | 0.18 | 0.97 | 0.82 | 1.80 | 2.88 | 0.74 | 0.86 | 0.95 | 0.88 | 1.05 | 1.79 |
| NZL00075 | 0.65 | 0.51 | 0.95 | 0.88 | 1.48 | 2.31 | 0.81 | 0.82 | 0.94 | 0.93 | 0.84 | 1.71 |
| PAK00006 | -0.17 | 0.72 | 0.80 | 1.15 | 1.13 | 5.87 | 0.57 | 0.60 | 0.77 | 0.97 | 0.67 | 3.57 |
| THA00002 | -0.92 | 0.44 | 0.47 | 1.06 | 1.17 | 3.36 | -0.73 | 0.39 | 0.55 | 0.92 | 0.6 | 3.19 |
| THA00015 | -3.16 | 0.25 | 0.31 | 1.16 | 0.77 | 5.47 | -0.1 | 0.42 | 0.62 | 0.94 | 0.57 | 2.82 |
| Europe | | | | | | | | | | | | |
| CHE00001 | 0.29 | 0.36 | 0.84 | 0.81 | 1.59 | 2.65 | 0.48 | 0.64 | 0.94 | 1.13 | 1.33 | 2.26 |
| CHE00002 | 0.96 | 0.91 | 0.98 | 0.99 | 1.09 | 1.12 | 0.80 | 0.89 | 0.9 | 0.94 | 1.00 | 2.57 |
| CHE00003 | 0.94 | 0.83 | 0.98 | 0.95 | 1.16 | 1.34 | 0.79 | 0.85 | 0.92 | 0.9 | 1.08 | 2.55 |
| DEU00001 | 0.88 | 0.83 | 0.96 | 0.96 | 1.16 | 1.94 | 0.74 | 0.85 | 0.88 | 0.97 | 1.09 | 2.85 |
| DEU00002 | 0.76 | 0.68 | 0.94 | 0.89 | 1.29 | 2.81 | 0.61 | 0.7 | 0.89 | 0.84 | 1.23 | 3.56 |
| DEU00003 | 0.83 | 0.75 | 0.95 | 0.91 | 1.22 | 2.46 | 0.63 | 0.73 | 0.92 | 0.80 | 1.16 | 3.62 |
| DEU00006 | 0.82 | 0.83 | 0.93 | 0.96 | 1.15 | 2.5 | 0.74 | 0.84 | 0.91 | 0.87 | 0.98 | 3.00 |
| ESP00008 | 0.54 | 0.78 | 0.78 | 1.02 | 1.02 | 4.31 | 0.89 | 0.93 | 0.95 | 0.97 | 0.96 | 2.10 |
| ESP00011 | 0.47 | 0.70 | 0.90 | 1.11 | 1.26 | 4.28 | 0.78 | 0.87 | 0.91 | 1.02 | 1.09 | 2.75 |
| ESP00012 | 0.57 | 0.80 | 0.82 | 1.05 | 1.07 | 4.33 | 0.82 | 0.90 | 0.91 | 1.02 | 0.97 | 2.78 |
| ESP00013 | 0.47 | 0.58 | 0.85 | 0.94 | 1.39 | 4.05 | 0.63 | 0.75 | 0.93 | 0.86 | 1.20 | 3.38 |
| FRA00006 | 0.88 | 0.90 | 0.96 | 1.03 | 1.09 | 2.16 | 0.86 | 0.86 | 0.95 | 0.93 | 0.89 | 2.36 |
| FRA00007 | 0.80 | 0.88 | 0.94 | 1.10 | 1.04 | 2.91 | 0.86 | 0.80 | 0.94 | 0.97 | 0.82 | 2.43 |
| FRA00015 | 0.86 | 0.84 | 0.95 | 1.00 | 1.16 | 2.12 | 0.88 | 0.89 | 0.95 | 0.95 | 1.09 | 2.02 |
| GBR00001 | -0.03 | 0.66 | 0.84 | 1.28 | 1.07 | 5.45 | 0.89 | 0.87 | 0.97 | 0.92 | 0.90 | 1.80 |
| GBR00004 | 0.13 | 0.70 | 0.81 | 1.21 | 1.08 | 4.75 | 0.73 | 0.84 | 0.91 | 0.87 | 0.96 | 2.66 |
| HUN00002 | 0.89 | 0.94 | 0.95 | 1.03 | 1.01 | 2.23 | 0.91 | 0.88 | 0.96 | 1.07 | 0.91 | 2.00 |
| NLD00001 | 0.94 | 0.86 | 0.98 | 0.96 | 1.13 | 1.50 | 0.85 | 0.86 | 0.97 | 0.87 | 0.97 | 2.35 |
| POL00006 | 0.81 | 0.82 | 0.96 | 1.17 | 0.98 | 3.19 | 0.94 | 0.80 | 0.98 | 1.00 | 0.80 | 1.80 |
| PRT00001 | 0.42 | 0.72 | 0.89 | 1.10 | 1.24 | 3.46 | 0.79 | 0.86 | 0.89 | 1.02 | 0.91 | 2.18 |
| North America | | | | | | | | | | | | |
| CAN00005 | 0.72 | 0.76 | 0.86 | 0.96 | 0.81 | 3.99 | 0.80 | 0.76 | 0.89 | 1.06 | 0.80 | 3.44 |
| CAN00006 | 0.86 | 0.91 | 0.93 | 1.05 | 0.96 | 3.20 | 0.92 | 0.81 | 0.96 | 1.06 | 0.83 | 2.52 |
| CAN00007 | 0.47 | 0.53 | 0.84 | 0.70 | 1.33 | 3.99 | 0.79 | 0.82 | 0.94 | 0.84 | 0.94 | 2.48 |
| CAN00052 | 0.75 | 0.70 | 0.90 | 0.81 | 1.22 | 4.30 | 0.85 | 0.83 | 0.94 | 0.90 | 0.87 | 3.26 |
| USA00007 | 0.89 | 0.89 | 0.96 | 1.09 | 0.95 | 2.96 | 0.89 | 0.83 | 0.95 | 1.03 | 0.84 | 2.98 |
| USA00011 | 0.20 | 0.49 | 0.95 | 1.13 | 1.49 | 4.29 | 0.67 | 0.82 | 0.95 | 1.10 | 1.14 | 2.74 |
| USA00012 | 0.90 | 0.86 | 0.98 | 1.12 | 0.93 | 2.78 | 0.92 | 0.81 | 0.97 | 1.01 | 0.82 | 2.50 |
| Russia | | | | | | | | | | | | |
| RUS00004 | 0.95 | 0.97 | 0.97 | 1.01 | 0.99 | 1.79 | 0.90 | 0.82 | 0.96 | 1.09 | 0.85 | 2.48 |
| RUS00005 | 0.46 | 0.69 | 0.77 | 0.90 | 1.18 | 4.62 | 0.89 | 0.93 | 0.95 | 0.94 | 0.99 | 2.06 |

continued on next page

| Station | WaterGAP | | | | | | Regression Model | | | | | |
|----------------------|----------|-------|------|---------|----------|------|------------------|------|------|---------|----------|------|
| | NSE | KGE | r | β | γ | RMSE | NSE | KGE | r | β | γ | RMSE |
| RUS00008 | 0.81 | 0.82 | 0.95 | 1.05 | 1.17 | 3.00 | 0.67 | 0.79 | 0.89 | 1.14 | 0.90 | 3.96 |
| RUS00011 | 0.88 | 0.90 | 0.94 | 0.97 | 0.93 | 2.33 | 0.82 | 0.78 | 0.92 | 0.96 | 0.80 | 2.90 |
| RUS00012 | 0.88 | 0.86 | 0.94 | 1.06 | 0.89 | 2.02 | 0.85 | 0.63 | 0.94 | 1.22 | 0.71 | 2.25 |
| RUS00015 | 0.76 | 0.85 | 0.90 | 1.00 | 1.11 | 4.19 | 0.88 | 0.87 | 0.94 | 1.05 | 0.89 | 3.01 |
| RUS00018 | 0.70 | 0.40 | 0.90 | 1.52 | 0.72 | 2.75 | 0.63 | 0.55 | 0.83 | 1.33 | 0.75 | 3.06 |
| RUS00028 | 0.03 | -0.13 | 0.83 | 2.07 | 0.68 | 4.34 | 0.54 | 0.42 | 0.84 | 1.51 | 0.77 | 3.00 |
| RUS00043 | 0.89 | 0.87 | 0.95 | 0.96 | 0.89 | 2.60 | 0.88 | 0.75 | 0.95 | 1.05 | 0.75 | 2.67 |
| South America | | | | | | | | | | | | |
| ARG00005 | -1.12 | 0.27 | 0.69 | 1.10 | 1.65 | 4.98 | -0.02 | 0.48 | 0.69 | 0.96 | 1.41 | 3.46 |
| ARG00012 | 0.41 | 0.87 | 0.95 | 1.11 | 1.05 | 3.10 | 0.77 | 0.78 | 0.90 | 0.97 | 0.81 | 1.91 |
| BRA00018 | -2.03 | 0.26 | 0.46 | 1.10 | 0.50 | 3.21 | -0.27 | 0.00 | 0.31 | 0.96 | 0.27 | 2.08 |
| BRA00086 | -0.10 | 0.60 | 0.75 | 1.14 | 0.73 | 4.17 | 0.55 | 0.65 | 0.77 | 0.97 | 0.73 | 2.67 |
| BRA00123 | -2.29 | 0.16 | 0.41 | 1.10 | 0.41 | 3.26 | -0.98 | 0.07 | 0.47 | 0.93 | 0.24 | 2.52 |
| BRA02104 | -0.42 | 0.79 | 0.82 | 1.10 | 1.02 | 2.99 | 0.40 | 0.59 | 0.76 | 0.96 | 0.67 | 1.94 |
| BRA02112 | 0.09 | 0.81 | 0.83 | 1.08 | 1.04 | 2.58 | 0.57 | 0.77 | 0.80 | 0.97 | 0.89 | 1.76 |

Table 3.3.: The worldwide median and average values of the NSE, KGE and RMSE for the simulation with WaterGAP and the regression model by PUNZET ET AL. (2012).

| Value | WaterGAP | | | | | | Regression Model | | | | | |
|---------------------------|----------|------|------|---------|----------|------|------------------|------|------|---------|----------|------|
| | NSE | KGE | r | β | γ | RMSE | NSE | KGE | r | β | γ | RMSE |
| worldwide | | | | | | | | | | | | |
| Median | 0.61 | 0.74 | 0.92 | 1.06 | 1.09 | 3.19 | 0.79 | 0.81 | 0.93 | 0.97 | 0.89 | 2.59 |
| Average | 0.01 | 0.65 | 0.83 | 1.08 | 1.08 | 3.64 | 0.59 | 0.70 | 0.85 | 0.99 | 0.86 | 2.65 |
| Asia & Oceania | | | | | | | | | | | | |
| Median | -0.27 | 0.53 | 0.89 | 1.09 | 1.17 | 3.29 | 0.78 | 0.77 | 0.94 | 0.95 | 0.81 | 2.61 |
| Average | -0.92 | 0.52 | 0.74 | 1.11 | 1.14 | 4.49 | 0.36 | 0.62 | 0.78 | 0.97 | 0.78 | 2.64 |
| Europe | | | | | | | | | | | | |
| Median | 0.81 | 0.81 | 0.94 | 1.01 | 1.14 | 2.73 | 0.80 | 0.86 | 0.93 | 0.95 | 0.98 | 2.49 |
| Average | 0.66 | 0.77 | 0.91 | 1.02 | 1.16 | 2.98 | 0.78 | 0.83 | 0.93 | 0.95 | 1.02 | 2.55 |
| North America | | | | | | | | | | | | |
| Median | 0.75 | 0.76 | 0.93 | 1.05 | 0.96 | 3.99 | 0.85 | 0.82 | 0.95 | 1.03 | 0.84 | 2.74 |
| Average | 0.68 | 0.73 | 0.92 | 0.98 | 1.10 | 3.64 | 0.83 | 0.81 | 0.94 | 1.00 | 0.89 | 2.85 |
| Russia | | | | | | | | | | | | |
| Median | 0.81 | 0.85 | 0.94 | 1.01 | 0.93 | 2.75 | 0.85 | 0.78 | 0.94 | 1.09 | 0.80 | 2.90 |
| Average | 0.71 | 0.69 | 0.91 | 1.17 | 0.95 | 3.07 | 0.78 | 0.73 | 0.91 | 1.14 | 0.82 | 2.82 |
| South America | | | | | | | | | | | | |
| Median | -0.42 | 0.6 | 0.75 | 1.10 | 1.02 | 3.21 | 0.40 | 0.59 | 0.76 | 0.96 | 0.73 | 2.08 |
| Average | -0.78 | 0.54 | 0.70 | 1.10 | 0.91 | 3.47 | 0.15 | 0.48 | 0.67 | 0.96 | 0.72 | 2.33 |

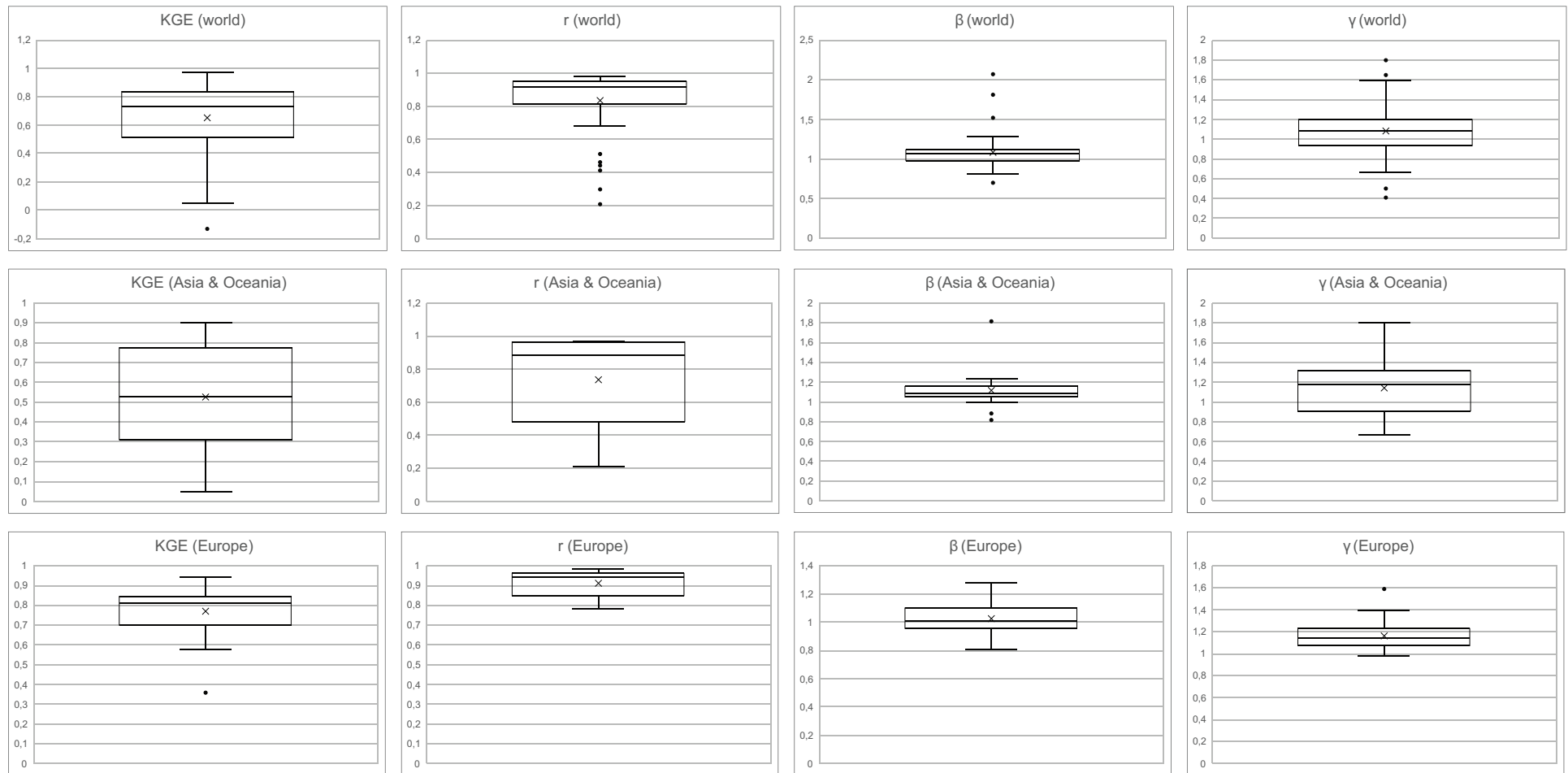


Figure 3.1.: The boxplots of the KGE, r , β and γ for the whole world and for five of the six geographic zones excluding Africa. The average is represented by the \times . The black dots are outliers. (continued in fig. 3.2)

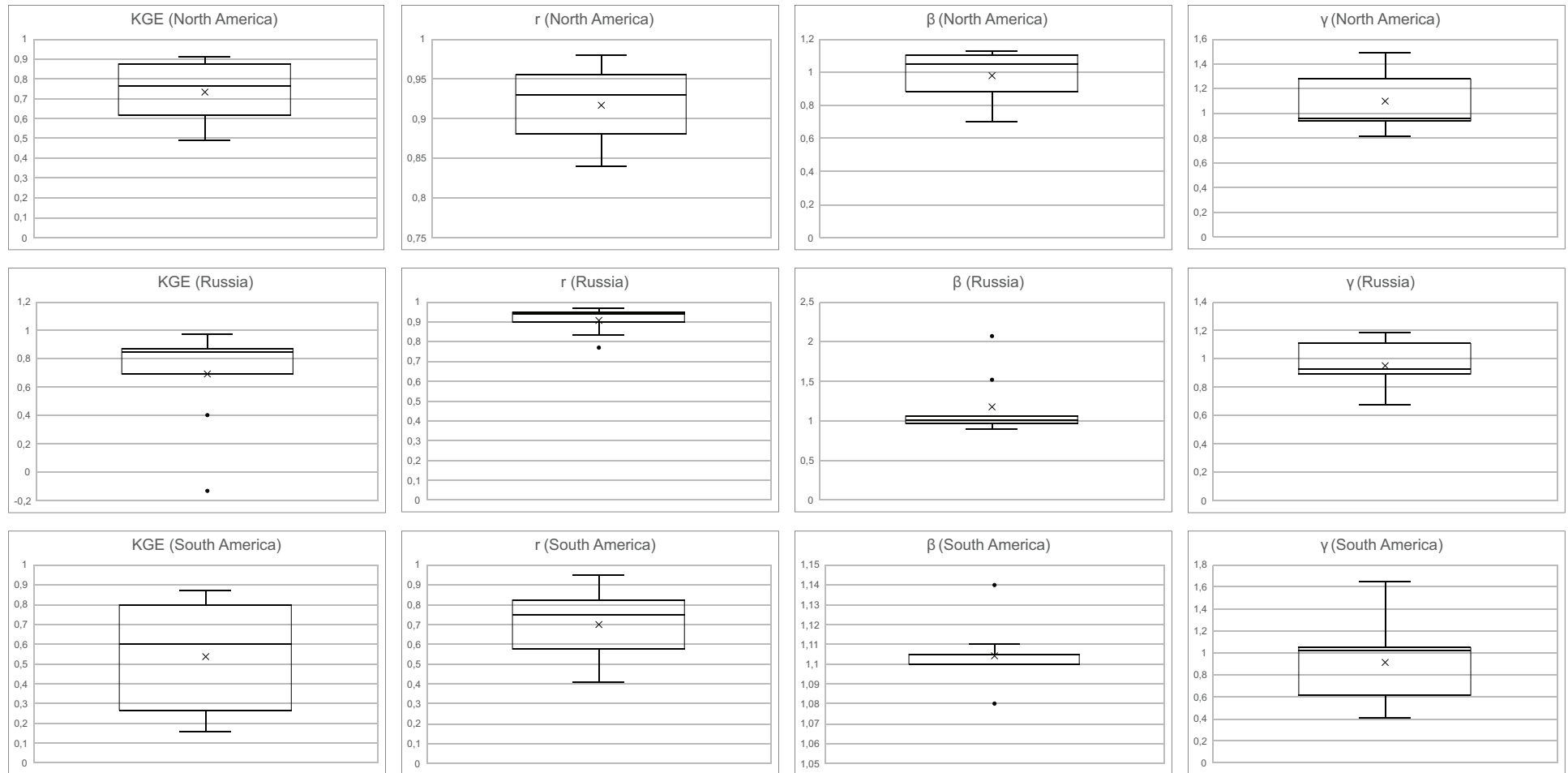


Figure 3.2.: The continuation of fig. 3.1 of the boxplots of the KGE, r , β and γ for the whole world and for five of the six geographic zones excluding Africa.

3.3. Other Validation Runs

Because the river Rhine has the best dataset of measured water temperatures, its stations (see fig. 3.3) are used to showcase the results for the other validation runs, except for runs where other stations are explicitly mentioned, for various reasons. However, all 62 stations are analyzed for every run, and all results can be found in the appendix A.1.1 of this thesis.

3.3.1. Groundwater Variations

This section shows the results for the different groundwater runs. The results of the run, where the groundwater temperature equals 10 °C, can be found in the appendix A.1.1. The standard run where the groundwater temperature equals the yearly mean air temperature is displayed on the right side for comparison. For a comparison with the regression model, see table 3.2.

Groundwater 4 °C

Table 3.4 shows the simulation results with the groundwater temperature equaling 4 °C for all Rhine stations. The results of this assumption are worse compared to the standard run.

Table 3.4.: The results for the simulation with the groundwater temperature equaling 4 °C for all Rhine stations and the standard run where the groundwater temperature equals the yearly mean air temperature.

| Station | Groundwater 4 °C | | | | | | Standard run | | | | | |
|----------|------------------|------|------|---------|----------|------|--------------|------|------|---------|----------|------|
| | NSE | KGE | r | β | γ | RMSE | NSE | KGE | r | β | γ | RMSE |
| CHE00001 | 0.22 | 0.41 | 0.79 | 0.84 | 1.53 | 2.79 | 0.29 | 0.36 | 0.84 | 0.81 | 1.59 | 2.65 |
| CHE00002 | 0.95 | 0.84 | 0.98 | 0.96 | 1.16 | 1.30 | 0.96 | 0.91 | 0.98 | 0.99 | 1.09 | 1.12 |
| CHE00003 | 0.91 | 0.72 | 0.99 | 0.91 | 1.26 | 1.70 | 0.94 | 0.83 | 0.98 | 0.95 | 1.16 | 1.34 |
| DEU00001 | 0.85 | 0.72 | 0.96 | 0.92 | 1.27 | 2.22 | 0.88 | 0.83 | 0.96 | 0.96 | 1.16 | 1.94 |
| DEU00002 | 0.66 | 0.52 | 0.95 | 0.84 | 1.44 | 3.32 | 0.76 | 0.68 | 0.94 | 0.89 | 1.29 | 2.81 |
| DEU00003 | 0.75 | 0.59 | 0.96 | 0.86 | 1.38 | 2.95 | 0.83 | 0.75 | 0.95 | 0.91 | 1.22 | 2.46 |
| DEU00006 | 0.78 | 0.68 | 0.94 | 0.90 | 1.29 | 2.76 | 0.82 | 0.83 | 0.93 | 0.96 | 1.15 | 2.50 |
| NLD00001 | 0.89 | 0.71 | 0.98 | 0.90 | 1.27 | 2.00 | 0.94 | 0.86 | 0.98 | 0.96 | 1.13 | 1.50 |

Groundwater max. 25 °C

In table 3.5 the simulation results for a groundwater temperature equaling the yearly mean air temperature with a maximum of 25 °C for all river Rhine stations can be seen. The results are not different to the standard run. The groundwater in the catchment area of the Rhine seems not to reach 25 °C. To show the influence of this assumption, stations located at the Mekong (KHM00003, KHM00006) and the Amazon (BRA00123) are shown in table 3.6. The results are better but only marginal.

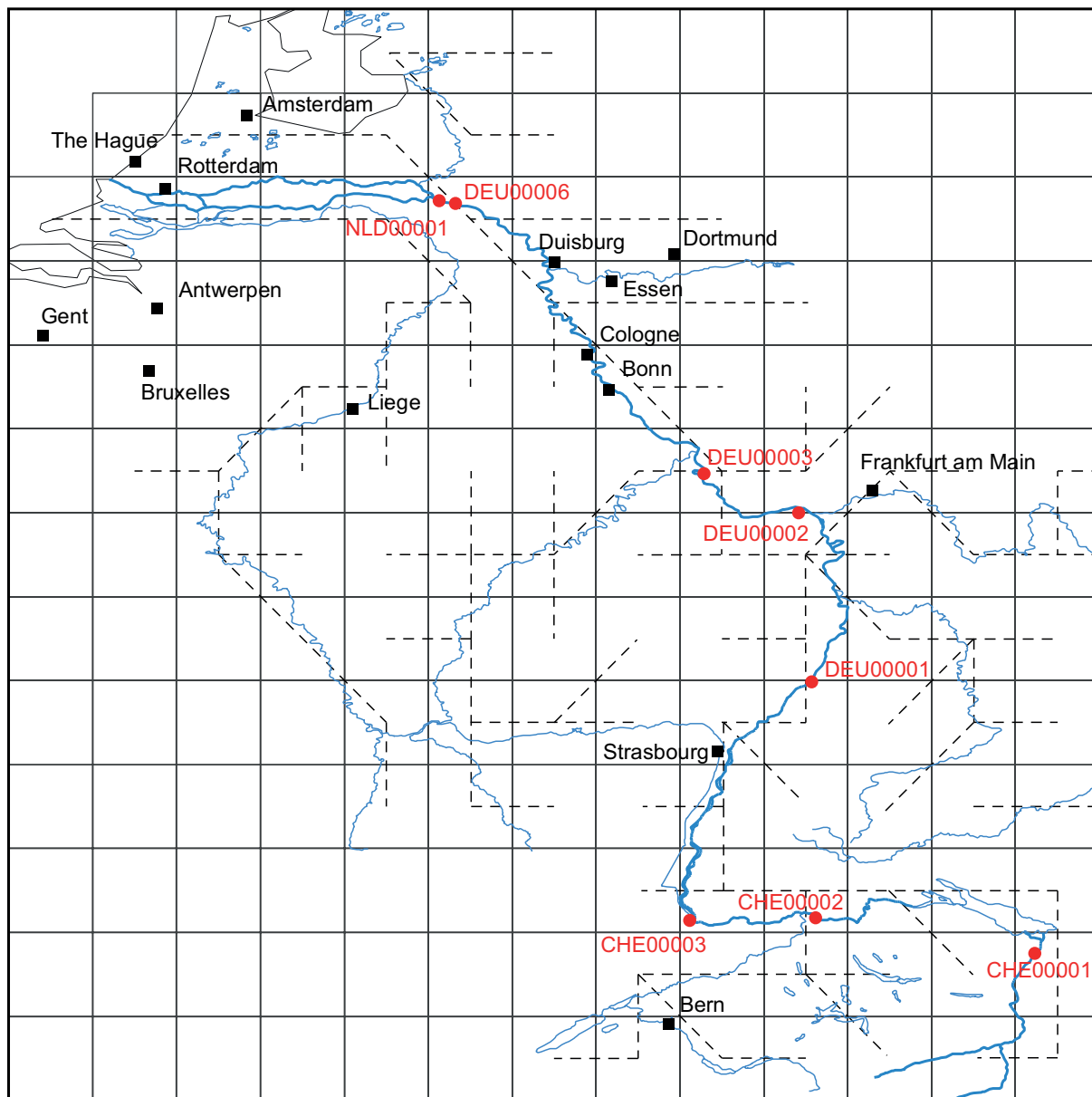


Figure 3.3.: The location of all measuring stations (red) along the Rhine (blue), including other rivers flowing into the Rhine, bigger cities (black) and the WaterGAP grid. The dashed lines represent the flow of the rivers in the WaterGAP model.

Table 3.5.: The results for the simulation with the groundwater temperature equaling the yearly mean air temperature with a maximum of 25 °C for all Rhine stations and the standard run where the groundwater temperature equals the yearly mean air temperature.

| Station | Groundwater max. 25 °C | | | | | | Standard run | | | | | |
|----------|------------------------|------|------|---------|----------|------|--------------|------|------|---------|----------|------|
| | NSE | KGE | r | β | γ | RMSE | NSE | KGE | r | β | γ | RMSE |
| CHE00001 | 0.29 | 0.36 | 0.84 | 0.81 | 1.59 | 2.65 | 0.29 | 0.36 | 0.84 | 0.81 | 1.59 | 2.65 |
| CHE00002 | 0.96 | 0.91 | 0.98 | 0.99 | 1.09 | 1.12 | 0.96 | 0.91 | 0.98 | 0.99 | 1.09 | 1.12 |
| CHE00003 | 0.94 | 0.83 | 0.98 | 0.95 | 1.16 | 1.34 | 0.94 | 0.83 | 0.98 | 0.95 | 1.16 | 1.34 |
| DEU00001 | 0.88 | 0.83 | 0.96 | 0.96 | 1.16 | 1.94 | 0.88 | 0.83 | 0.96 | 0.96 | 1.16 | 1.94 |
| DEU00002 | 0.76 | 0.68 | 0.94 | 0.89 | 1.29 | 2.81 | 0.76 | 0.68 | 0.94 | 0.89 | 1.29 | 2.81 |
| DEU00003 | 0.83 | 0.75 | 0.95 | 0.91 | 1.22 | 2.46 | 0.83 | 0.75 | 0.95 | 0.91 | 1.22 | 2.46 |
| DEU00006 | 0.82 | 0.83 | 0.93 | 0.96 | 1.15 | 2.50 | 0.82 | 0.83 | 0.93 | 0.96 | 1.15 | 2.50 |
| NLD00001 | 0.94 | 0.86 | 0.98 | 0.96 | 1.13 | 1.50 | 0.94 | 0.86 | 0.98 | 0.96 | 1.13 | 1.50 |

Table 3.6.: The results for the simulation with the groundwater temperature equaling the yearly mean air temperature with a maximum of 25 °C for the Mekong (KHM00003, KHM00006) and the Amazon (BRA00123) stations and the standard run where the groundwater temperature equals the yearly mean air temperature.

| Station | Groundwater max. 25 °C | | | | | | Standard run | | | | | |
|----------|------------------------|------|------|---------|----------|------|--------------|------|------|---------|----------|------|
| | NSE | KGE | r | β | γ | RMSE | NSE | KGE | r | β | γ | RMSE |
| KHM00003 | -0.35 | 0.70 | 0.73 | 1.06 | 0.88 | 2.05 | -0.38 | 0.70 | 0.74 | 1.06 | 0.86 | 2.08 |
| KHM00006 | -0.87 | 0.28 | 0.29 | 1.05 | 0.89 | 2.64 | -0.88 | 0.28 | 0.30 | 1.05 | 0.88 | 2.65 |
| BRA00123 | -2.25 | 0.16 | 0.40 | 1.10 | 0.42 | 3.24 | -2.29 | 0.16 | 0.41 | 1.10 | 0.41 | 3.26 |

3.3.2. Power Plant Cooling

This section shows the different power plant cooling runs. The two other runs, where the cooling water is discharged into the rivers with the river temperature +5 °C and a temperature of 30 °C, can be found in the appendix A.1.1. For a comparison with the standard run where the cooling water is discharged into the rivers with the river temperature +3 °C, see the right side of the tables. To compare the results to the regression model, see table 3.2.

Power Plant Cooling +10 °C

Table 3.7 shows the the power plant cooling run results, where the cooling water is discharged into the rivers with the river temperature +10 °C. This assumption shows mixed results for the NSE depending on the station positions. For example, DEU00002 and DEU00003 are better, but DEU00001 is worse. The KGE indicates better results throughout. The RMSE is only worse for DEU00001.

No Power Plant Cooling

Table 3.8 shows the results if power plant cooling is not considered. All the results are worse, considering the strong human influence on the Rhine.

Table 3.7.: The results for power plant cooling with resulting water temperature equaling the river temperature +10 °C. (standard run +3 °C)

| Station | Power plant cooling +10 °C | | | | | | Standard run | | | | | |
|----------|----------------------------|------|------|---------|----------|------|--------------|------|------|---------|----------|------|
| | NSE | KGE | r | β | γ | RMSE | NSE | KGE | r | β | γ | RMSE |
| CHE00001 | 0.30 | 0.37 | 0.84 | 0.81 | 1.58 | 2.64 | 0.29 | 0.36 | 0.84 | 0.81 | 1.59 | 2.65 |
| CHE00002 | 0.96 | 0.94 | 0.98 | 1.01 | 1.06 | 1.10 | 0.96 | 0.91 | 0.98 | 0.99 | 1.09 | 1.12 |
| CHE00003 | 0.95 | 0.86 | 0.98 | 0.97 | 1.13 | 1.22 | 0.94 | 0.83 | 0.98 | 0.95 | 1.16 | 1.34 |
| DEU00001 | 0.87 | 0.92 | 0.96 | 1.06 | 1.03 | 2.02 | 0.88 | 0.83 | 0.96 | 0.96 | 1.16 | 1.94 |
| DEU00002 | 0.84 | 0.83 | 0.94 | 0.97 | 1.16 | 2.28 | 0.76 | 0.68 | 0.94 | 0.89 | 1.29 | 2.81 |
| DEU00003 | 0.87 | 0.86 | 0.95 | 0.98 | 1.13 | 2.16 | 0.83 | 0.75 | 0.95 | 0.91 | 1.22 | 2.46 |
| DEU00006 | 0.82 | 0.91 | 0.92 | 1.03 | 1.04 | 2.48 | 0.82 | 0.83 | 0.93 | 0.96 | 1.15 | 2.50 |
| NLD00001 | 0.94 | 0.96 | 0.98 | 1.03 | 1.03 | 1.42 | 0.94 | 0.86 | 0.98 | 0.96 | 1.13 | 1.50 |

Table 3.8.: The results for the simulation without power plant cooling. (standard run +3 °C)

| Station | No power plant cooling | | | | | | Standard run | | | | | |
|----------|------------------------|------|------|---------|----------|------|--------------|------|------|---------|----------|------|
| | NSE | KGE | r | β | γ | RMSE | NSE | KGE | r | β | γ | RMSE |
| CHE00001 | 0.29 | 0.36 | 0.84 | 0.81 | 1.59 | 2.65 | 0.29 | 0.36 | 0.84 | 0.81 | 1.59 | 2.65 |
| CHE00002 | 0.96 | 0.90 | 0.98 | 0.98 | 1.10 | 1.15 | 0.96 | 0.91 | 0.98 | 0.99 | 1.09 | 1.12 |
| CHE00003 | 0.94 | 0.81 | 0.98 | 0.94 | 1.18 | 1.41 | 0.94 | 0.83 | 0.98 | 0.95 | 1.16 | 1.34 |
| DEU00001 | 0.85 | 0.76 | 0.95 | 0.92 | 1.22 | 2.19 | 0.88 | 0.83 | 0.96 | 0.96 | 1.16 | 1.94 |
| DEU00002 | 0.69 | 0.61 | 0.94 | 0.85 | 1.36 | 3.16 | 0.76 | 0.68 | 0.94 | 0.89 | 1.29 | 2.81 |
| DEU00003 | 0.80 | 0.70 | 0.95 | 0.89 | 1.27 | 2.67 | 0.83 | 0.75 | 0.95 | 0.91 | 1.22 | 2.46 |
| DEU00006 | 0.80 | 0.77 | 0.93 | 0.93 | 1.21 | 2.62 | 0.82 | 0.83 | 0.93 | 0.96 | 1.15 | 2.50 |
| NLD00001 | 0.92 | 0.80 | 0.98 | 0.92 | 1.19 | 1.73 | 0.94 | 0.86 | 0.98 | 0.96 | 1.13 | 1.50 |

3.3.3. No Ice Formation

Table 3.9 shows the simulation results without ice formation in surface water bodies. For a comparison with the standard run, where ice can form, see the right side of the table. To compare the results with the regression model results, look at table 3.2. Compared to the standard run, all results are worse. The changes in water temperature and, therefore, the coefficients compared to the standard run are most likely not due to the Rhine itself, but due to its inflows.

Table 3.9.: The results for the simulation run without ice formation. (standard run with ice formation)

| Station | No ice formation | | | | | | Standard run | | | | | |
|----------|------------------|------|------|---------|----------|------|--------------|------|------|---------|----------|------|
| | NSE | KGE | r | β | γ | RMSE | NSE | KGE | r | β | γ | RMSE |
| CHE00001 | 0.29 | 0.10 | 0.94 | 0.76 | 1.86 | 2.64 | 0.29 | 0.36 | 0.84 | 0.81 | 1.59 | 2.65 |
| CHE00002 | 0.93 | 0.84 | 0.98 | 0.97 | 1.15 | 1.46 | 0.96 | 0.91 | 0.98 | 0.99 | 1.09 | 1.12 |
| CHE00003 | 0.91 | 0.77 | 0.98 | 0.94 | 1.22 | 1.65 | 0.94 | 0.83 | 0.98 | 0.95 | 1.16 | 1.34 |
| DEU00001 | 0.85 | 0.77 | 0.95 | 0.95 | 1.22 | 2.19 | 0.88 | 0.83 | 0.96 | 0.96 | 1.16 | 1.94 |
| DEU00002 | 0.71 | 0.61 | 0.93 | 0.88 | 1.37 | 3.10 | 0.76 | 0.68 | 0.94 | 0.89 | 1.29 | 2.81 |
| DEU00003 | 0.80 | 0.69 | 0.95 | 0.90 | 1.29 | 2.68 | 0.83 | 0.75 | 0.95 | 0.91 | 1.22 | 2.46 |
| DEU00006 | 0.79 | 0.76 | 0.93 | 0.95 | 1.23 | 2.68 | 0.82 | 0.83 | 0.93 | 0.96 | 1.15 | 2.50 |
| NLD00001 | 0.93 | 0.79 | 0.98 | 0.95 | 1.21 | 1.62 | 0.94 | 0.86 | 0.98 | 0.96 | 1.13 | 1.50 |

3.3.4. No Water Use

Table 3.10 shows the results for a simulation without human water use. The standard run, where human water use is considered, is displayed on the right side. For comparison with the regression model, see table 3.2. All results are equal or worse except for the NSE of CHE00001.

Table 3.10.: The results for a simulation without consideration of human water use. (standard run human use considered)

| Station | No water use | | | | | | Standard run | | | | | |
|----------|--------------|------|------|---------|----------|------|--------------|------|------|---------|----------|------|
| | NSE | KGE | r | β | γ | RMSE | NSE | KGE | r | β | γ | RMSE |
| CHE00001 | 0.33 | 0.35 | 0.86 | 0.80 | 1.61 | 2.58 | 0.29 | 0.36 | 0.84 | 0.81 | 1.59 | 2.65 |
| CHE00002 | 0.96 | 0.90 | 0.98 | 0.98 | 1.10 | 1.14 | 0.96 | 0.91 | 0.98 | 0.99 | 1.09 | 1.12 |
| CHE00003 | 0.94 | 0.82 | 0.98 | 0.94 | 1.17 | 1.38 | 0.94 | 0.83 | 0.98 | 0.95 | 1.16 | 1.34 |
| DEU00001 | 0.85 | 0.76 | 0.96 | 0.92 | 1.22 | 2.16 | 0.88 | 0.83 | 0.96 | 0.96 | 1.16 | 1.94 |
| DEU00002 | 0.71 | 0.61 | 0.94 | 0.86 | 1.36 | 3.11 | 0.76 | 0.68 | 0.94 | 0.89 | 1.29 | 2.81 |
| DEU00003 | 0.8 | 0.71 | 0.95 | 0.89 | 1.27 | 2.63 | 0.83 | 0.75 | 0.95 | 0.91 | 1.22 | 2.46 |
| DEU00006 | 0.81 | 0.78 | 0.93 | 0.93 | 1.20 | 2.59 | 0.82 | 0.83 | 0.93 | 0.96 | 1.15 | 2.50 |
| NLD00001 | 0.92 | 0.81 | 0.98 | 0.93 | 1.18 | 1.69 | 0.94 | 0.86 | 0.98 | 0.96 | 1.13 | 1.50 |

3.3.5. No Precipitation Cooling

Table 3.11 shows the simulation results if the precipitation is not cooled down by 1.5 °C, which automatically does not cool down the surface runoff as well, because the two water temperatures are always equal. The standard run, where the precipitation is cooled by 1.5 °C, is shown on the right side of the table. For comparison with the regression model, see table 3.2. All results of this run indicate a slightly better performance of the model for the Rhine.

Table 3.11.: The results, if the precipitation and the surface runoff are not cooled down. (standard run cooled by 1.5 °C)

| Station | No precipitation cooling | | | | | | Standard run | | | | | |
|----------|--------------------------|------|------|---------|----------|------|--------------|------|------|---------|----------|------|
| | NSE | KGE | r | β | γ | RMSE | NSE | KGE | r | β | γ | RMSE |
| CHE00001 | 0.29 | 0.45 | 0.80 | 0.85 | 1.49 | 2.66 | 0.29 | 0.36 | 0.84 | 0.81 | 1.59 | 2.65 |
| CHE00002 | 0.96 | 0.93 | 0.98 | 1.00 | 1.07 | 1.09 | 0.96 | 0.91 | 0.98 | 0.99 | 1.09 | 1.12 |
| CHE00003 | 0.95 | 0.85 | 0.98 | 0.95 | 1.14 | 1.27 | 0.94 | 0.83 | 0.98 | 0.95 | 1.16 | 1.34 |
| DEU00001 | 0.89 | 0.85 | 0.96 | 0.96 | 1.14 | 1.89 | 0.88 | 0.83 | 0.96 | 0.96 | 1.16 | 1.94 |
| DEU00002 | 0.76 | 0.70 | 0.94 | 0.88 | 1.27 | 2.78 | 0.76 | 0.68 | 0.94 | 0.89 | 1.29 | 2.81 |
| DEU00003 | 0.83 | 0.77 | 0.95 | 0.91 | 1.20 | 2.42 | 0.83 | 0.75 | 0.95 | 0.91 | 1.22 | 2.46 |
| DEU00006 | 0.83 | 0.84 | 0.93 | 0.95 | 1.13 | 2.43 | 0.82 | 0.83 | 0.93 | 0.96 | 1.15 | 2.50 |
| NLD00001 | 0.94 | 0.88 | 0.98 | 0.95 | 1.11 | 1.48 | 0.94 | 0.86 | 0.98 | 0.96 | 1.13 | 1.50 |

3.3.6. Natural Run

Table 3.12 shows the results for a natural run, which means that human water use and reservoirs are not considered. Because there are no reservoirs in the catchment of the river Rhine, two

stations in Brazil (BRA02104 and BRA02112) are used. Otherwise, the results would be the same as with no human water use considered (see table 3.10). The standard run results, where human water use and reservoirs are considered, are shown for a better comparison. The results for the regression model can be seen in table 3.2. The results show that the rivers are, in reality, influenced by anthropogenic effects because the results are worse than the standard run. One exception is the NSE of BRA02104. This might be due to the non-consideration of reservoirs when also compared to the no reservoir run (see chapter 3.3.7).

Table 3.12.: Results for a simulation of a natural run (without human water use and reservoirs considered) for two stations in Brazil

| Station | Natural run | | | | | | Standard run | | | | | |
|----------|-------------|------|------|---------|----------|------|--------------|------|------|---------|----------|------|
| | NSE | KEG | r | β | γ | RMSE | NSE | KEG | r | β | γ | RMSE |
| BRA02104 | -0.25 | 0.60 | 0.61 | 1.07 | 0.96 | 2.81 | -0.42 | 0.79 | 0.82 | 1.10 | 1.02 | 2.99 |
| BRA02112 | -0.30 | 0.59 | 0.63 | 1.06 | 1.16 | 3.09 | 0.09 | 0.81 | 0.83 | 1.08 | 1.04 | 2.58 |

3.3.7. No Reservoirs

Table 3.13 shows the results for a run without consideration of reservoirs. Reservoirs are then treated as global lakes by WaterGAP. Because there are no reservoirs in the catchment of the river Rhine, two stations in Brazil (BRA02104 and BRA02112), which are located directly behind two different reservoirs, are used. The standard run results, where reservoirs are considered, are also shown for a better comparison. The regression model results can be seen in table 3.2 for comparison. The KGE is worse, which indicates that the reservoir calculation leads to better results than the global lake calculation if a reservoir is present in reality. However, the NSE indicates better results for BRA02104 when no reservoir is considered there.

Table 3.13.: The results for a simulation without reservoirs considered for two stations in Brazil.

| Station | No reservoirs | | | | | | Standard run | | | | | |
|----------|---------------|------|------|---------|----------|------|--------------|------|------|---------|----------|------|
| | NSE | KEG | r | β | γ | RMSE | NSE | KEG | r | β | γ | RMSE |
| BRA02104 | -0.27 | 0.60 | 0.61 | 1.07 | 0.96 | 2.83 | -0.42 | 0.79 | 0.82 | 1.10 | 1.02 | 2.99 |
| BRA02112 | -0.26 | 0.60 | 0.63 | 1.06 | 1.14 | 3.03 | 0.09 | 0.81 | 0.83 | 1.08 | 1.04 | 2.58 |

3.4. Sensitivity Analysis

A sensitivity analysis (see eq. 2.7) is done for one station for each geographic region mentioned before. The examined input values are the groundwater temperature, the temperature increase of the discharged water used for cooling power plants and the precipitation and surface runoff temperature decrease due to the rainfall originating higher up in the atmosphere. The results are shown in table 3.14. The model shows a small positive sensitivity for the groundwater

temperature and the cooling water temperature increase. The sensitivity for precipitation and surface runoff temperature decrease is slightly negative for SDN00002 and NLD00001. Generally, the influence of the three input values on the results is relatively low between 0.00 and 0.16. The groundwater temperature seems to have the most influence for all stations. For the station SDN00002, the performance of WaterGAP must be considered, which is not the best with an NSE of -2 and a KGE of 0.55 (see table 3.2).

Table 3.14.: The sensitivity analysis of the WaterGAP model for the groundwater temperature, the power plant discharge temperature and the precipitation and surface runoff temperature.

| Station | Variable | Sensitivity |
|----------|--|-------------|
| SDN00002 | Groundwater temperature | 0.00 |
| | Precip. & Surface runoff temperature decrease | -0.26 |
| | Power plant cooling water temperature increase | 0.00 |
| CHN00002 | Groundwater temperature | 0.03 |
| | Precip. & Surface runoff temperature decrease | 0.01 |
| | Power plant cooling water temperature increase | 0.00 |
| NLD00001 | Groundwater temperature | 0.16 |
| | Precip. & Surface runoff temperature decrease | -0.08 |
| | Power plant cooling water temperature increase | 0.13 |
| CAN00006 | Groundwater temperature | 0.06 |
| | Precip. & Surface runoff temperature decrease | 0.03 |
| | Power plant cooling water temperature increase | 0.03 |
| RUS00011 | Groundwater temperature | 0.14 |
| | Precip. & Surface runoff temperature decrease | 0.05 |
| | Power plant cooling water temperature increase | 0.02 |
| ARG00012 | Groundwater temperature | 0.01 |
| | Precip. & Surface runoff temperature decrease | 0.01 |
| | Power plant cooling water temperature increase | 0.00 |

3.5. Simulation of the Future

The following table and figures are intended to show future changes in water temperature in the context of climate change compared to the mean of the period from 1961 to 1990 (see fig. 3.5), the currently valid climatological reference period (WMO 2017). For all four scenarios, RCP2.6 (fig. 3.6), RCP4.5 (fig. 3.7), RCP6 (fig. 3.8) and RCP8.5 (fig. 3.9) of the IPSL-CM5A-LR (PIK n.d.) climate forcing the mean water temperature for every cell for the years 2071 to 2099 was calculated using the standard run. Only the human water use and the power plant cooling was not considered. Table 3.15 and figure 3.4 illustrate the change of the continental area fraction with specific water temperature ranges due to climate change. The total continental area in WaterGAP is 134,579,721.79 km². The temperature ranges of 0 – 10 °C and 20 – 30 °C decrease for every scenario. The 30 – 40 °C temperature range increases sig-

nificantly, especially for scenario RCP8.5. The range of 10 – 20 °C stays relatively constant. The shift from 0 – 10 °C to 10 – 20 °C is clearly visible around the Baltic Sea and Russia. The change from 20 – 30 °C to 30 – 40 °C is most prominent in Australia, India, in Africa south of the Sahara, especially the Congo Basin, Central America and the Amazon. The cells, where no water temperature data could be computed due to insufficient water, increase, clearly visible in the northeast of Africa.

Table 3.15.: The continental area in [%] with corresponding water temperature range to show the climate change impact, while no data indicates no water temperature could be computed. Scenario historic: mean water temperature between 1961 to 1990 and Scenarios RCP: mean water temperature between 2071-2099 (also see fig 3.4)

| Scenario | 0-10 °C | 10-20 °C | 20-30 °C | 30-40 °C | 40-50 °C | 50-60 °C | no data |
|----------|---------|----------|----------|----------|----------|----------|---------|
| historic | 33.44 | 23.06 | 37.32 | 5.69 | 0.26 | 0.00 | 0.24 |
| RCP2.6 | 28.72 | 23.00 | 34.76 | 12.77 | 0.44 | 2.29E-05 | 0.30 |
| RCP4.5 | 26.33 | 23.62 | 32.95 | 16.25 | 0.53 | 2.29E-05 | 0.32 |
| RCP6 | 25.64 | 23.52 | 32.36 | 17.46 | 0.55 | 2.29E-05 | 0.47 |
| RCP8.5 | 20.74 | 24.68 | 28.05 | 25.16 | 0.88 | 4.47E-3 | 0.49 |

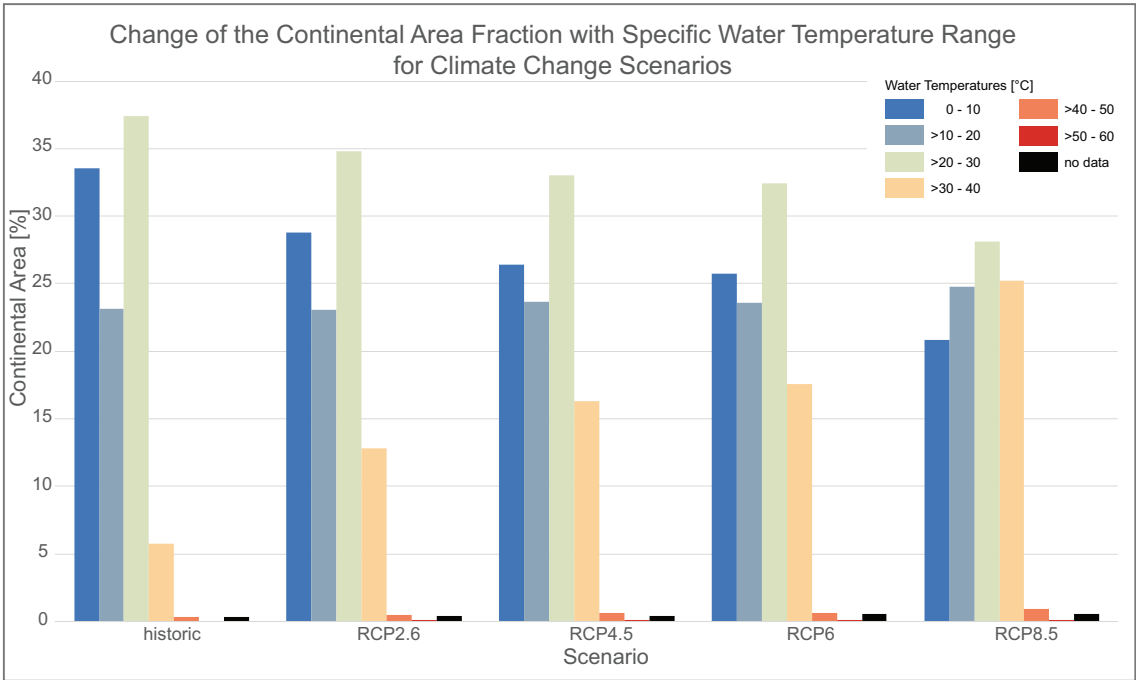


Figure 3.4.: The continental area in [%] with corresponding water temperature range to show the climate change impact, while no data indicates no water temperature could be computed. Scenario historic: mean water temperature between 1961 to 1990 and Scenarios RCP: mean water temperature between 2071-2099 (also see table 3.15)

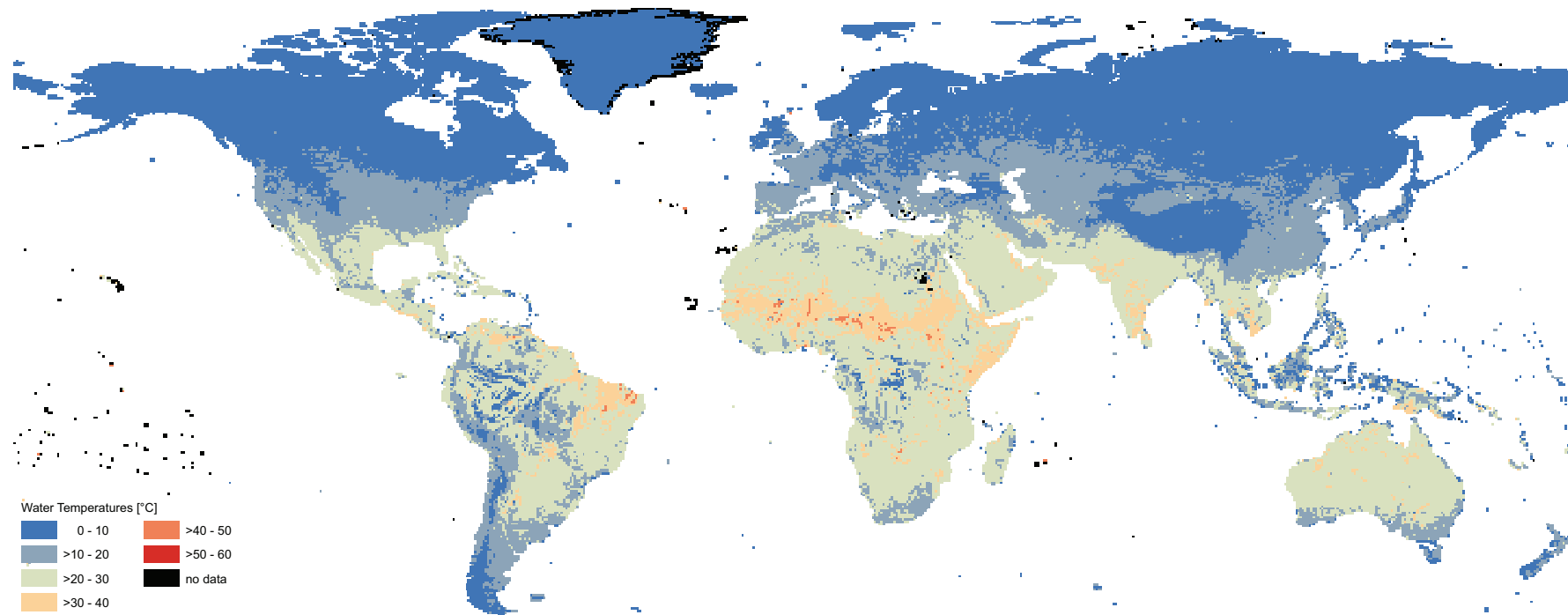


Figure 3.5.: The worldwide water temperature mean for the time period 1961 to 1990 for comparison.

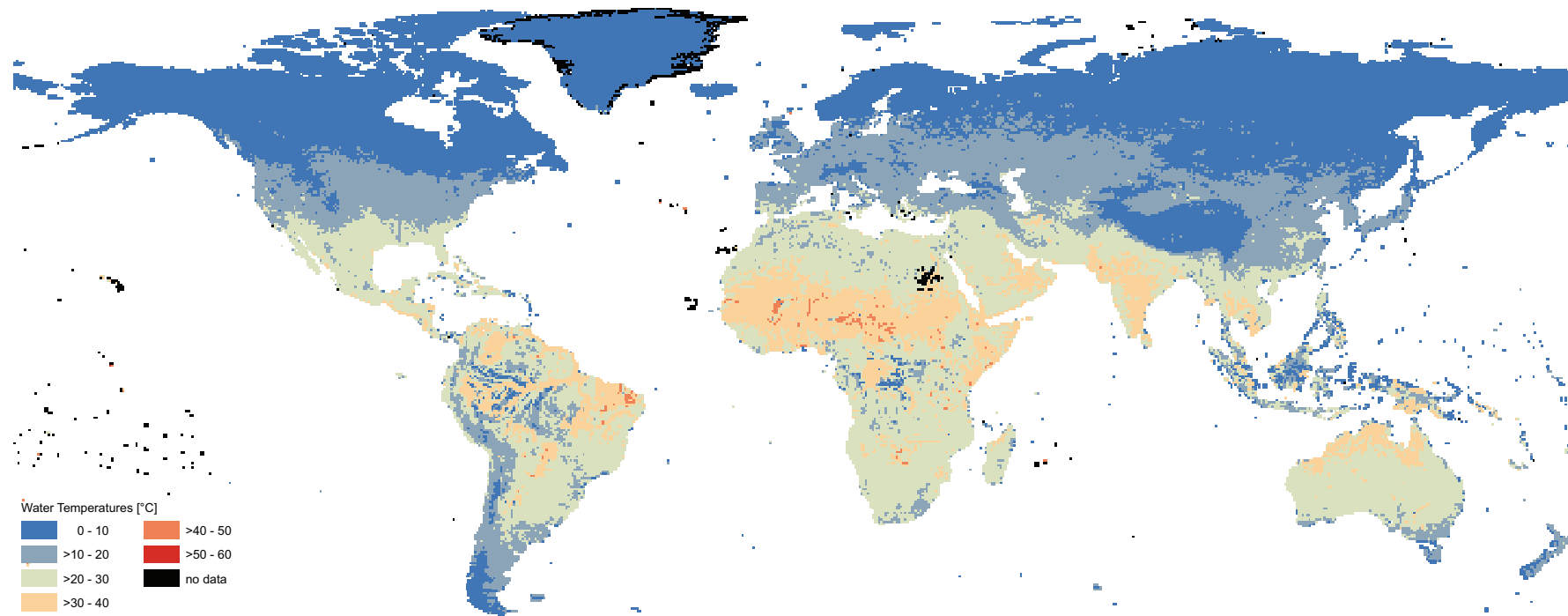


Figure 3.6.: The worldwide water temperature mean for the time period 2071 to 2099 for the RCP2.6 scenario.

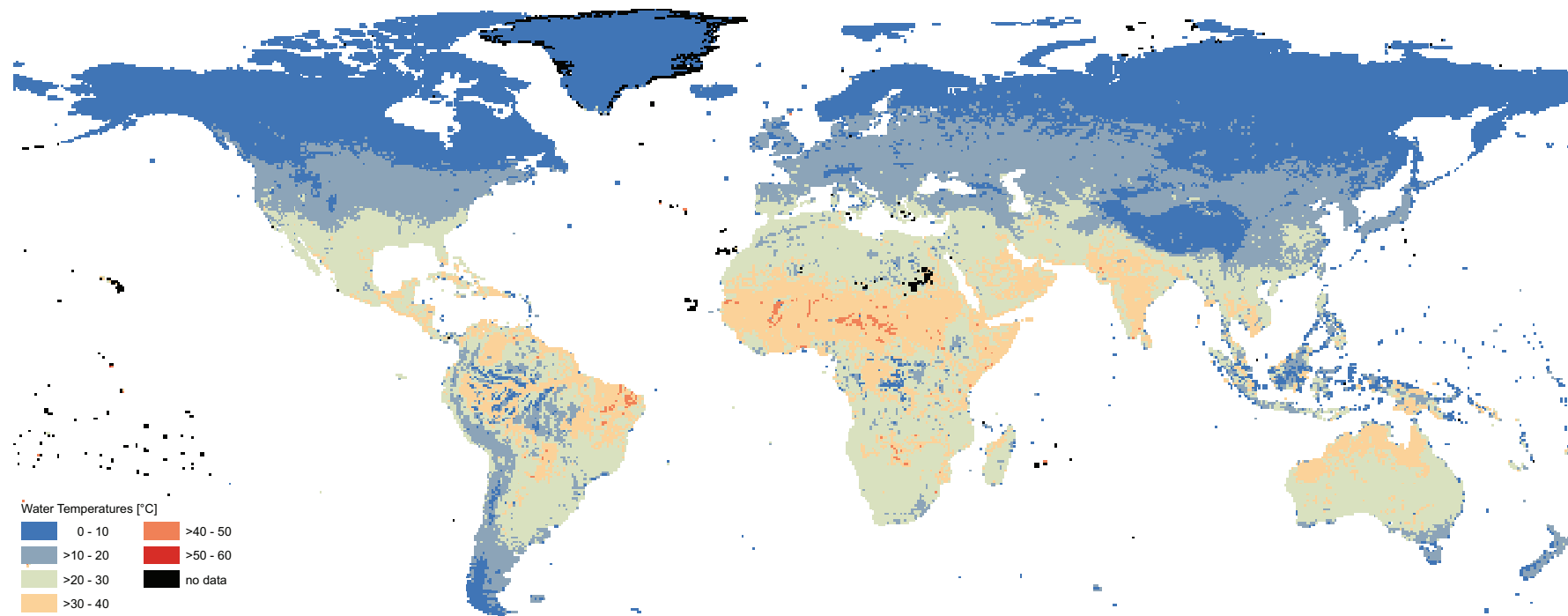


Figure 3.7.: The worldwide water temperature mean for the time period 2071 to 2099 for the RCP4.5 scenario.

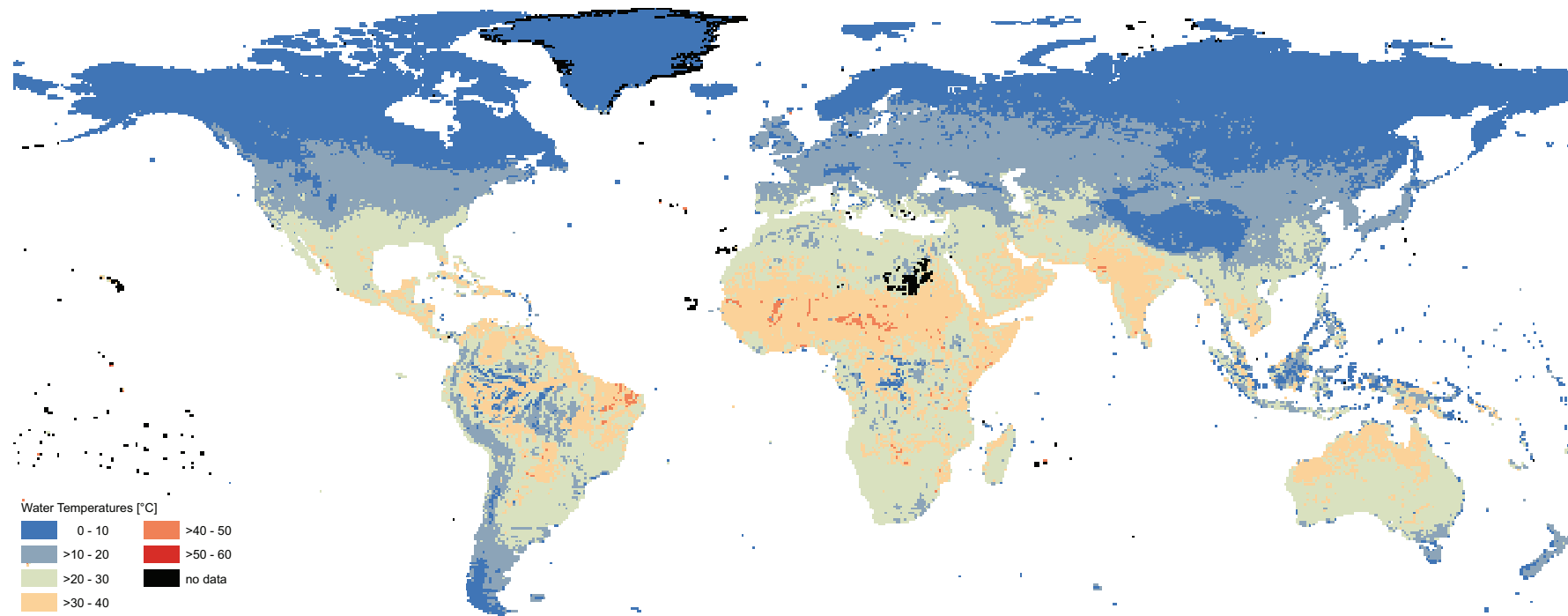


Figure 3.8.: The worldwide water temperature mean for the time period 2071 to 2099 for the RCP6 scenario.

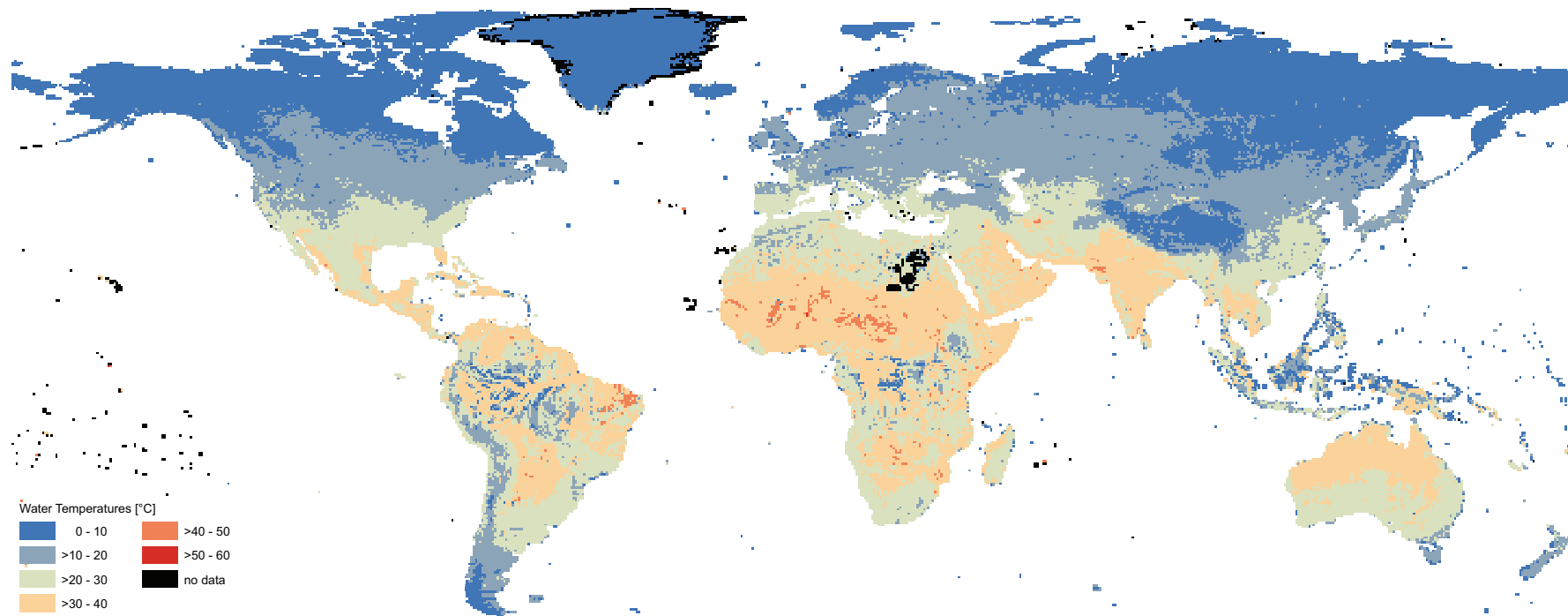


Figure 3.9.: The worldwide water temperature mean for the time period 2071 to 2099 for the RCP8.5 scenario.

4. Discussion, Analysis and Interpretation of Results

4.1. Influence of Observed Data Availability on Validation

The availability, quantity and quality of real-world data have an impact on the validation results. The Rhine stations DEU00006 and NLD00001 are within one grid cell of WaterGAP, without another river flowing into the Rhine in between these two stations in reality (see fig. 3.3). Therefore, those two stations are beneficial to demonstrate the impact of data availability on the validation. NLD00001 has measured water temperature data two to four times per month (see table 4.3) while DEU00006 only has data for every one to two months and a data gap of four years (see table 4.2). The mean of the measured values of NLD00001 is computed for validation, which is also done for the daily WaterGAP model data. The differences are shown in table 4.1. The same model data seem to be less accurate for the station DEU00006 than for NLD00001. If only few data samples are available, the observed data's monthly mean value is inaccurate compared to the mean of 30 or 31 model values per month. This influences the NSE and KGE computations. Another factor influencing the validation results is the station's position relative to other rivers flowing into the evaluated river. If the estuary is downstream of the measuring station (see fig. 4.1), discrepancies occur compared to the model due to the computation timing. The water temperature is calculated at the end of the cell, where the inflow influences the result, whereas the observed data does not reflect the effects of the inflowing water. That is why at some measuring stations, the cell upstream of the station was chosen for comparison and computation of the NSE, KGE and RMSE. The same applies to the influence of power plants.

Table 4.1.: A comparison of the validation results for the stations DEU00006 and NLD00001, which are located in the same cell but have different quantities of measured data.

| Station | NSE | KGE | r | β | γ | RMSE |
|----------|------|------|------|---------|----------|------|
| DEU00006 | 0.82 | 0.83 | 0.93 | 0.96 | 1.15 | 2.50 |
| NLD00001 | 0.94 | 0.86 | 0.98 | 0.96 | 1.13 | 1.50 |

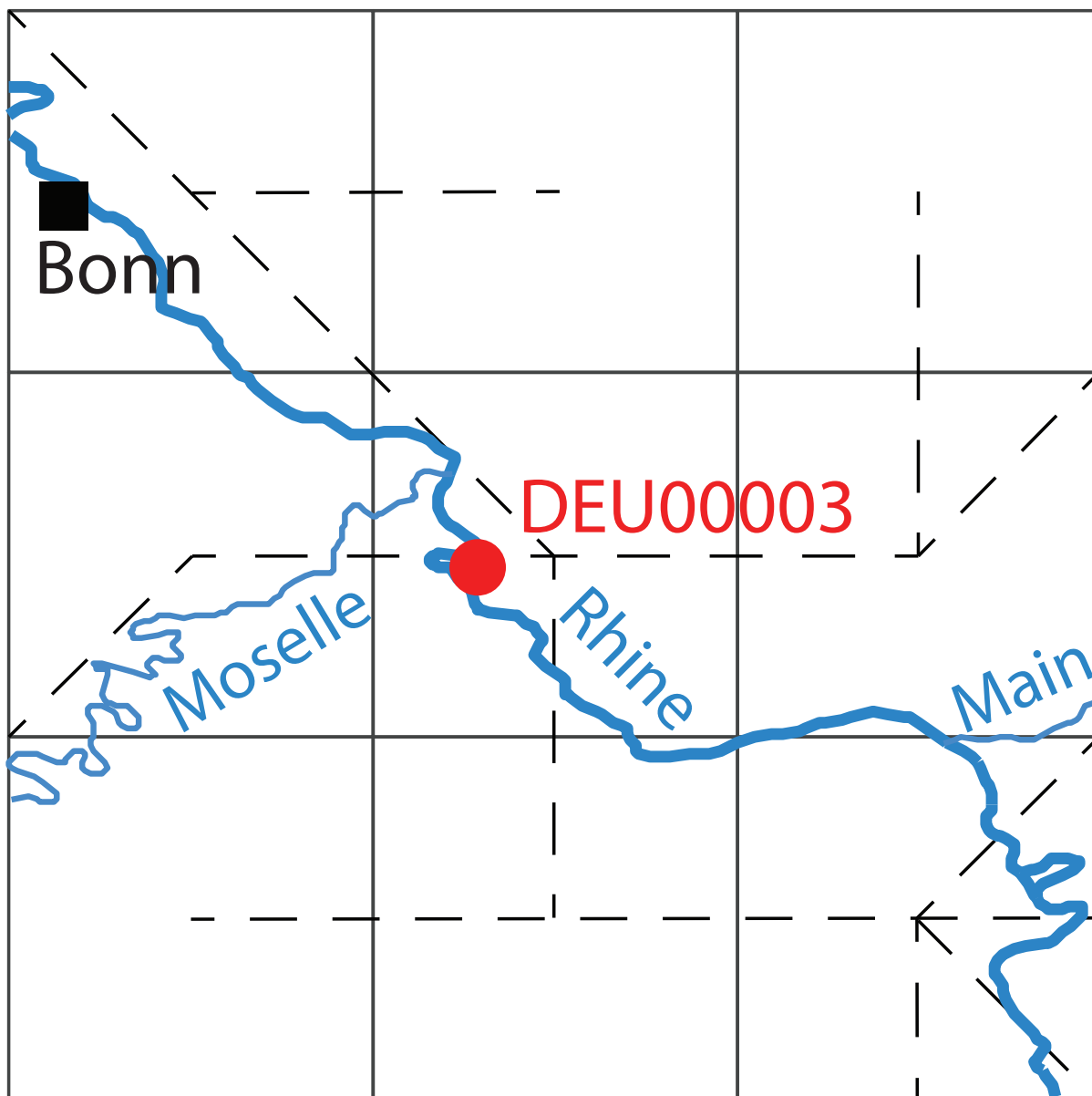


Figure 4.1.: An example for an estuary downstream of a measuring station. The river Moselle flowing into the Rhine.

Table 4.2.: The observed water temperature data [°C] for the Rhine measuring station DEU00006.

| | JAN | FEB | MAR | APR | MAY | JUN | JUL | AUG | SEP | OCT | NOV | DEC |
|------|------|------|-------|-------|-------|-------|-------|-------|-------|-------|-------|-------|
| 1979 | 4.40 | | 5.50 | | 11.20 | | 18.90 | | 19.70 | | 16.10 | 8.50 |
| 1980 | | 5.20 | | 8.90 | | 15.00 | | 17.50 | | 18.80 | 10.30 | |
| 1981 | | | | | | | | | | | | |
| 1982 | | | | | | | | | | | | |
| 1983 | | | | | | | | | | | | |
| 1984 | | | | | | | | | | | | |
| 1985 | | 2.50 | 5.80 | | 12.90 | | 18.70 | | 20.40 | | 15.60 | |
| 1986 | 7.40 | | 4.00 | 7.80 | | 16.20 | | 22.10 | | 17.80 | | 11.50 |
| 1987 | 4.85 | 3.80 | 4.87 | 11.00 | 14.15 | 15.95 | 19.45 | 19.60 | 20.20 | 15.05 | 11.90 | 7.15 |
| 1988 | 7.77 | 6.55 | 6.60 | 10.25 | 15.90 | 17.95 | 20.77 | 22.20 | 18.85 | 15.50 | 11.90 | 8.25 |
| 1989 | 7.75 | 7.30 | 10.00 | 12.20 | 16.20 | 11.80 | 22.00 | 20.60 | 19.90 | 20.10 | 15.70 | 7.35 |
| 1990 | 7.25 | 7.45 | 8.80 | 12.00 | 18.80 | 20.60 | 21.40 | 22.40 | 16.65 | 15.35 | 11.10 | 5.80 |
| 1991 | 6.90 | 3.10 | 8.00 | 10.90 | 14.15 | 18.70 | 23.00 | 21.20 | | 16.70 | 10.10 | 5.60 |
| 1992 | 6.70 | 5.40 | 8.40 | 11.55 | 20.80 | 20.10 | 23.50 | 21.30 | 18.80 | 14.00 | 10.90 | 8.50 |
| 1993 | 2.80 | 6.30 | 10.10 | 12.10 | 19.30 | 22.40 | 21.80 | 21.30 | 17.25 | 11.30 | 5.60 | 7.70 |
| 1994 | 6.50 | 6.10 | 8.55 | 12.60 | 15.50 | 19.00 | 23.80 | 21.00 | 18.20 | 14.00 | 12.70 | 9.00 |
| 1995 | 6.20 | 8.40 | 7.77 | 12.10 | 15.65 | 16.70 | 22.05 | 22.13 | 17.45 | 16.15 | 9.50 | 5.90 |

Table 4.3.: The observed water temperature data [°C] for the Rhine measuring station NLD00001.

| | JAN | FEB | MAR | APR | MAY | JUN | JUL | AUG | SEP | OCT | NOV | DEC |
|------|------|------|-------|-------|-------|-------|-------|-------|-------|-------|-------|------|
| 1979 | 2.64 | 4.20 | 7.50 | 10.57 | 14.38 | 19.80 | 20.00 | 19.84 | 18.45 | 15.85 | 10.08 | 8.22 |
| 1980 | 4.05 | 6.64 | 8.38 | 11.50 | 14.58 | 18.08 | 16.27 | 20.65 | 18.62 | 14.48 | 8.43 | 5.12 |
| 1981 | 4.28 | 4.77 | 8.53 | 12.30 | 16.73 | 18.85 | 19.32 | 20.27 | 18.64 | 12.15 | 9.35 | 4.64 |
| 1982 | 3.60 | 5.17 | 7.52 | 11.37 | 15.62 | 20.55 | 21.74 | 21.25 | 19.98 | 14.33 | 11.18 | 7.14 |
| 1983 | 6.80 | 5.10 | 8.06 | 10.33 | 14.35 | 18.14 | 23.38 | 22.74 | 18.05 | 15.17 | 10.45 | 6.50 |
| 1984 | 5.50 | 5.12 | 7.70 | 10.28 | 14.42 | 17.45 | 19.30 | 21.22 | 17.40 | 13.78 | 11.36 | 8.90 |
| 1985 | 3.70 | 4.03 | 7.40 | 11.20 | 16.33 | 17.88 | 20.28 | 20.25 | 18.65 | 15.92 | 8.07 | 8.63 |
| 1986 | 4.86 | 2.78 | 6.80 | 8.62 | 16.10 | 17.90 | 21.78 | 21.60 | 16.93 | 15.70 | 10.75 | 8.20 |
| 1987 | 2.97 | 4.43 | 5.62 | 10.43 | 14.00 | 15.05 | 20.44 | 19.30 | 18.80 | 14.18 | 11.00 | 7.16 |
| 1988 | 7.25 | 6.60 | 6.85 | 11.15 | 16.60 | 19.15 | 21.55 | 22.15 | 18.50 | 16.00 | 11.17 | 8.25 |
| 1989 | 7.75 | 8.10 | 9.40 | 11.35 | 16.50 | 21.60 | 23.50 | 22.55 | 19.80 | 15.80 | 11.47 | 6.45 |
| 1990 | 7.50 | 7.95 | 9.80 | 11.65 | 17.77 | 19.35 | 20.20 | 23.00 | 18.85 | 15.93 | 9.90 | 2.70 |
| 1991 | 6.25 | 4.10 | 10.15 | 12.30 | 14.80 | 18.25 | 23.00 | 22.45 | 21.00 | 14.60 | 9.25 | 6.20 |
| 1992 | 5.95 | 5.90 | 8.05 | 9.95 | 17.80 | 20.05 | 23.80 | 21.70 | 19.40 | | 10.60 | 8.15 |
| 1993 | 7.80 | 6.40 | 9.63 | 14.80 | 21.20 | 22.80 | 20.50 | 21.75 | 17.35 | 13.70 | 8.75 | 7.75 |
| 1994 | 6.90 | 5.55 | 9.43 | 13.80 | 17.10 | 18.25 | 25.17 | 23.08 | 18.55 | 13.38 | 13.05 | 9.38 |
| 1995 | 6.05 | 6.20 | 7.53 | 12.05 | 15.30 | 16.65 | 21.80 | 22.47 | 18.50 | 17.10 | 9.90 | 6.10 |

4.2. Standard Simulation Run

The median of the NSE and the KGE (see table 3.3) indicate a good performance ($0.5 < \text{NSE} < 0.65$ (RITTER & MUÑOZ-CARPENA 2013)) of the WaterGAP model worldwide. Exceptions are the geographic regions of South America and Asia & Oceania except the stations located in China. In general, in the warmer regions, the performance seems insufficient with great spans of KGE values for Asia & Oceania and South America (see fig. 3.1 and 3.2). The values of β are mostly greater than 1 in those regions (see table 3.2), indicating an overestimation. VAN BEEK ET AL. (2012) have identical problems with their model. They propose as possible causes the underestimation of the water albedo and emissivity, a possible overestimation of the incoming radiation due to the neglect of shading of the tropical rainforest canopy, especially for smaller streams and the assumption that rainfall has the same temperature as the atmosphere (VAN BEEK ET AL. 2012). Their last proposition was addressed by cooling the precipitation by 1.5 °C. The results show a small improvement (see appendix A.1.1) but indicate that this cooling is still not enough because rainfall in the tropics originates from higher up in the atmosphere. Also, the groundwater is estimated too warm by the assumption of using the yearly mean air temperature, as shown by the groundwater run, where the maximum temperature is set to 25 °C (see table 3.6), which yields slightly better results.

The station AUS00004 shows exceptionally poor results with an NSE of -12.61 and a KGE of 0.05. This may have several reasons. One might be the Lake Victoria situated nearby with its outflow, the Rufus River, directly upstream of the measuring station (see fig. 4.2). Perhaps the river is not completely mixed in reality at the location of the measuring station. Another reason could be that the water volume calculation of WaterGAP is not very accurate if the catchment area is small, which could lead to very small volumes. This hypothesis is backed by the significant changes in the water temperature calculated by WaterGAP for the no-human-use scenario and the scenario where the precipitation is not cooled (see table 4.4). In the no usage scenario the water volume in the cell is larger than in the standard run, which leads to significantly better results. The scenario with no precipitation cooling shows a significant impact of the small precipitation volume on the water temperature, which indicates a small water volume in the cell.

Table 4.4.: A comparison of three scenarios for the station AUS00004 indicating a small water volume in the cell of the station.

| Scenario | NSE | KGE | r | β | γ | RMSE |
|--------------------|--------|------|------|---------|----------|-------|
| Standard | -12.61 | 0.05 | 0.82 | 1.81 | 1.46 | 16.86 |
| No usage | -1.18 | 0.51 | 0.90 | 1.28 | 1.39 | 6.74 |
| No precip. cooling | -8.88 | 0.05 | 0.86 | 1.63 | 1.70 | 14.37 |



Figure 4.2.: The surroundings of station AUS00004. (source: Google Earth)

4.3. Other Validation Runs

The Rhine station CHE00001 shows poor results for every validation scenario. Perhaps unconsidered effects, which play a role in reality, are at play here, for example, glacial waters. The regression model also shows relatively poor results of an NSE of 0.48 and a KGE of 0.64 for the standard run, which usually are > 0.78 in Europe (see table 3.3).

4.3.1. Groundwater Variations

The results show that the assumption for the groundwater temperature equaling the yearly mean air temperature is better than a constant temperature of $4\text{ }^{\circ}\text{C}$. Exceptions are stations where the water temperature is overestimated, like in South America. Logically these stations show better results if the water temperature gets colder due to colder groundwater. The air temperatures are available anyhow because they are needed for WaterGAP. Thus an approach with a constant groundwater temperature is not feasible. The approach could be refined by setting a maximum groundwater temperature as done with the scenario "Groundwater max. $25\text{ }^{\circ}\text{C}$ " (see page 24). It has to be considered that a maximum temperature may be counterproductive if climate change scenarios are computed.

4.3.2. Power Plant Cooling

The scenario where the cooling water is discharged into the river with $+10\text{ }^{\circ}\text{C}$ seems to yield better results, at least for the Rhine (see table 3.7). Other stations like POL00006 (see table 4.5)

at the Odra River indicate a worsened performance, already with +5 °C (see appendix A.1.1). This may be due to the strong anthropogenic influences on the Rhine. For example, factories also use cooling water, which is not considered in the WaterGAP temperature calculation. It is difficult to improve the model in this area because every country has different legislation. For example, in Germany, the maximum allowed river temperature is dependent on the fish species. Hence, every power plant is subject to its own specific legal requirements depending on the location (see LANGE (2009)). The scenario without power plant cooling is only interesting for a naturalized simulation. It yields worse results (see table 3.8) if it is the goal to depict the reality.

Table 4.5.: A comparison of the standard run versus "power plant cooling +10 °C" scenario for the station POL00006.

| Scenario | NSE | KGE | r | β | γ | RMSE |
|----------------|------|------|------|---------|----------|------|
| Standard | 0.81 | 0.82 | 0.96 | 1.17 | 0.98 | 3.19 |
| cooling +10 °C | 0.73 | 0.69 | 0.96 | 1.27 | 0.86 | 3.77 |

4.3.3. No Ice Formation

The comparison of the standard scenario and the no-ice-formation scenario indicates mixed results. The data can be found in the appendix A.1.1. Especially for ice formation, the quality of the observed data and how it was measured play an important role. At the station CAN00005, the actual water temperature is measured in a depth of 1 m, whereas in Russia, the temperature is measured directly at the surface. This means if there is ice, the temperature automatically equals 0 °C. Varying results for the model's accuracy are produced because this data influence the NSE and KGE. Also, in Russia, the observed data has gaps during winter because no measuring was conducted. WaterGAP calculates the water temperature below the ice cover. If ice formation is turned off and the water temperature is negative, it is automatically set to 0 °C. This is the temperature often measured in Canada and Russia and, therefore, the coefficients indicate better results. The reason in Canada, which leads to worse results with ice formation turned on, might be too warm groundwater temperatures in the winter, caused by the assumption that the groundwater temperature equals the yearly mean air temperature. Overall the ice formation calculation is a source for improvement.

4.3.4. No Water Use

The scenario without human use is only interesting for a naturalized simulation. Generally, better results are achieved if the usage is incorporated into the simulation because anthropogenic effects influence many rivers. Nevertheless, sometimes it can lead to poor results if the water volume is getting too small due to the human use and the approach nears its limits. One example

is the station AUS00004 (see table 4.4), where a significant improvement can be seen if the water use is turned off.

4.3.5. No Precipitation Cooling

The results are better for the Rhine without cooling (see table 3.11). Perhaps 1.5 °C is too much cooling for the precipitation and surface runoff or, which is probably more likely the reason, the Rhine is heavily influenced by industries and power plants, which use the water and warm it up. The β value is smaller than 1 for every Rhine station, which indicates that WaterGAP underestimates the water temperature probably due to the mentioned anthropogenic effects. This, in return, leads to worse results if the precipitation and surface water runoff cool the Rhine. The other stations in Europe show similar behavior (see appendix A.1.1), and generally, the rivers in Europe are influenced by human water use. For stations in the warmer regions of the world, which nearly all have poor results to begin with, the cooling has a slight positive effect on the accuracy (see appendix A.1.1). The precipitation and, therefore, the surface runoff temperature for these regions must be cooled further than 1.5 °C to get better results because rainfall in the tropics originates from higher up in the atmosphere than, for example, in Europe. Perhaps two or three cooling coefficients, depending on the location in the world, should be considered.

4.3.6. Natural Run

This scenario can be used to show the impact of humanity on the water temperature. A comparison of the Rhine station NLD00001 for the natural run, the standard run and the observed real-world data can be seen in figure 4.3. The water temperature of the natural run is roughly 0.5 °C colder than the temperature of the standard run, which in turn is roughly 0.5 to 1 °C colder than the observed data. This indicates that the anthropogenic influences on the Rhine thus account for 1 to 1.5 °C.

4.3.7. No Reservoir

This run is useful for a naturalized scenario, but generally, better results are achieved if reservoirs are enabled (see table 3.13). WaterGAP treats reservoirs as global lakes if the reservoir calculation is deactivated. This means different water volume calculations are computed, and the water temperature is calculated with a different fetch length for the thermocline. Reservoirs use an equilateral triangle versus a square for global lakes (see chapter 2.1).

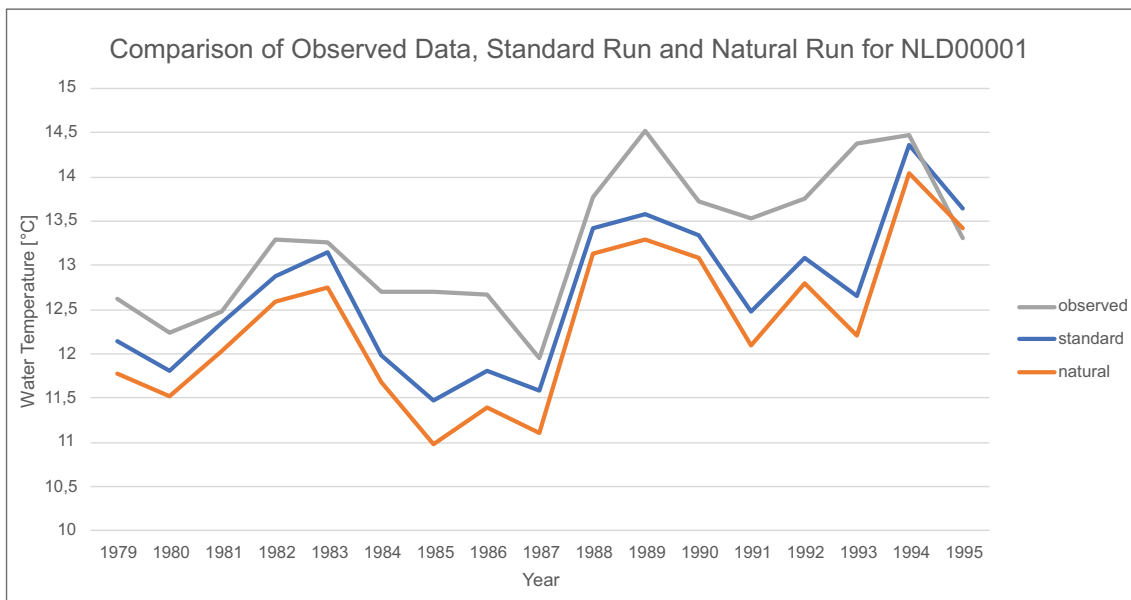


Figure 4.3.: A comparison of the observed data, the natural run and the standard run for the station NLD00001 to show the influence of anthropogenic effects on the water temperature.

4.4. Comparison of WaterGAP With the Regression Model of PUNZET ET AL. (2012) for Future Climate Scenarios

There is, of course, no observed data for the future. Therefore the WaterGAP model data without human water use and power plant cooling is compared with the regression model by PUNZET ET AL. (2012) in the time frame 2020 to 2099. The results for the four scenarios RCP2.6, RCP4.5, RCP6 and RCP8.5 for several stations are shown in figure 4.4 to 4.8. The assumption, expressed by CAISSIE (2006), that regression models perform worse if the environmental parameters change, because they are based on historical data, cannot be confirmed per se. Due to climate change, the environmental parameters do change, but the results are similar to the physics-based approach implemented in WaterGAP. In both, the water temperature rises relatively parallel to each other. Even in RCP8.5, where the environmental parameters change the most, the results are similar. Especially for CAN00006 and RUS00011 (fig. 4.6 and 4.7), WaterGAP and the regression model compute nearly identical results. Climate change has little impact due to the location on earth. However, especially for ARG00012 (see fig. 4.8), the trend lines diverge significantly at the end. This could indicate that the environmental parameters have changed enough near the end of the simulated period, so the regression model starts to underestimate the climate change impacts. Similar behavior, only less pronounced, can be seen for CHN00002 (see fig. 4.4), where the trend line of the regression model crosses the trend line of the air temperature around the year 2075. All selected stations indicate good performance of the WaterGAP model for historical climate data ($KGE > 0.81$). Therefore, the climate change scenarios should also perform well. The approximately 2 °C difference between the regression model and WaterGAP for ARG00012 (see fig. 4.8) could be due to the same problems of WaterGAP already mentioned in chapter 4.2.

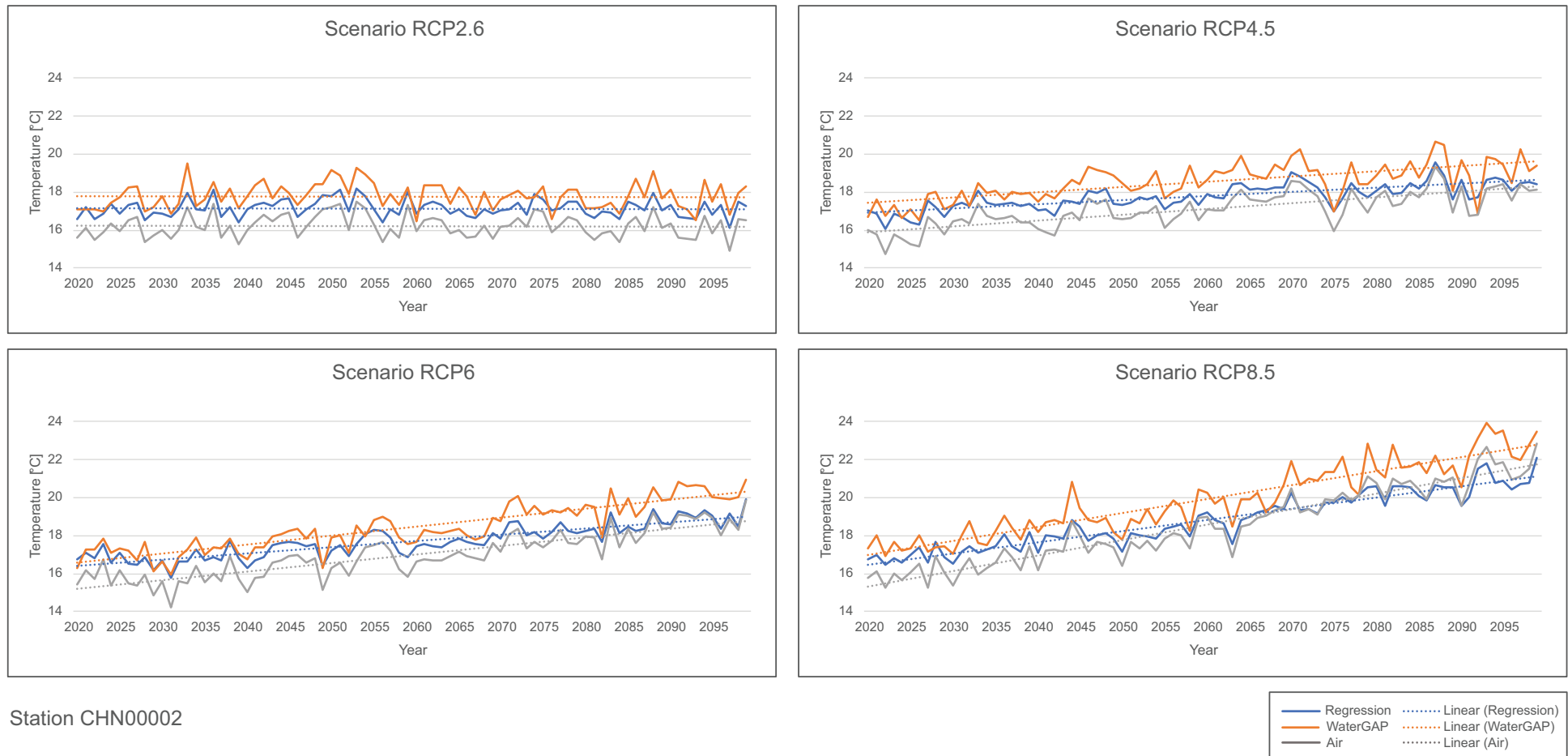


Figure 4.4.: A comparison of the scenarios RCP2.6, RCP4.5, RCP6 and RCP8.5 for the WaterGAP model without human use and power plant cooling and the regression model by PUNZET ET AL. (2012) between the years 2020 to 2099 for the station CHN00002.

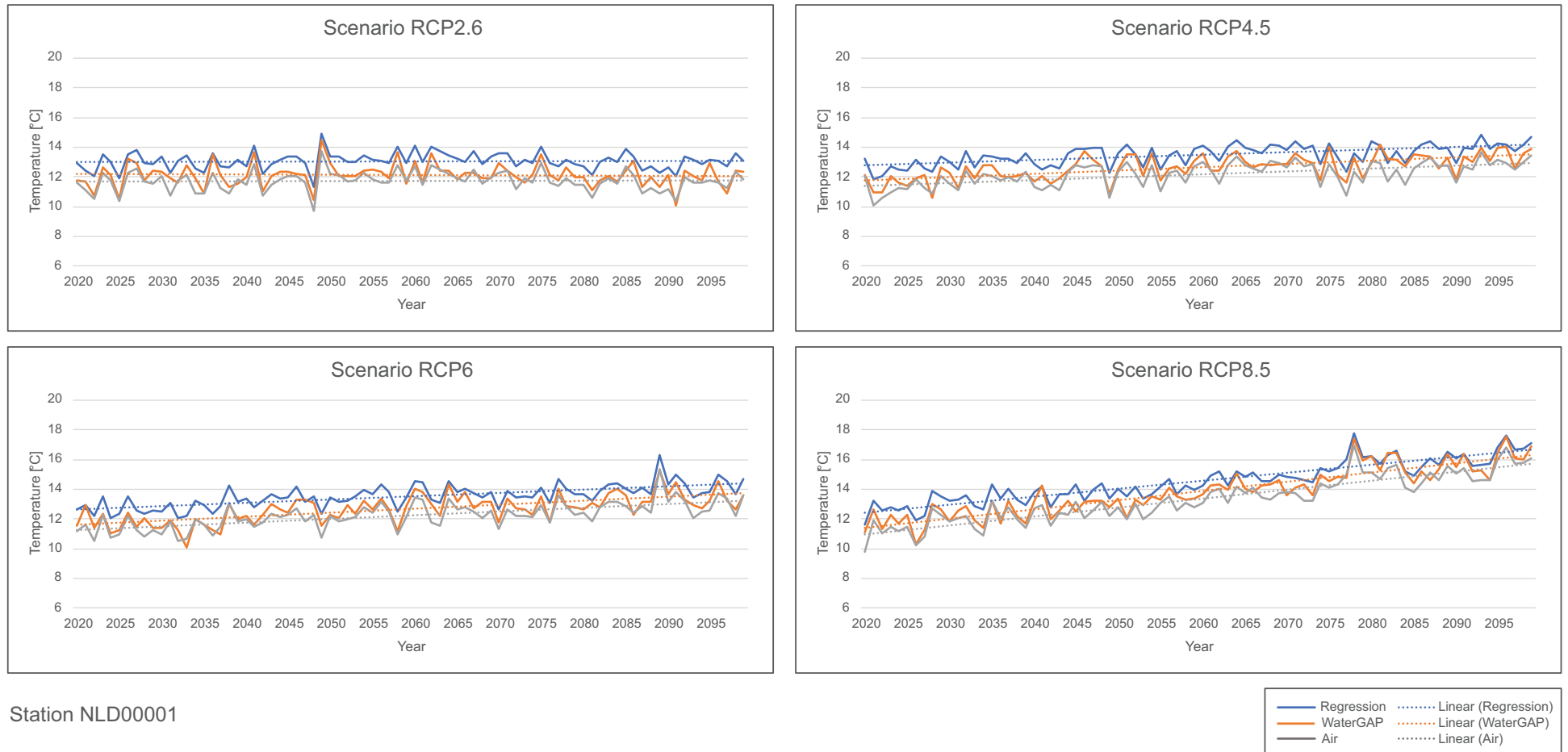


Figure 4.5.: A comparison of the scenarios RCP2.6, RCP4.5, RCP6 and RCP8.5 for the WaterGAP model without human use and power plant cooling and the regression model by PUNZET ET AL. (2012) between the years 2020 to 2099 for the station NLD00001.

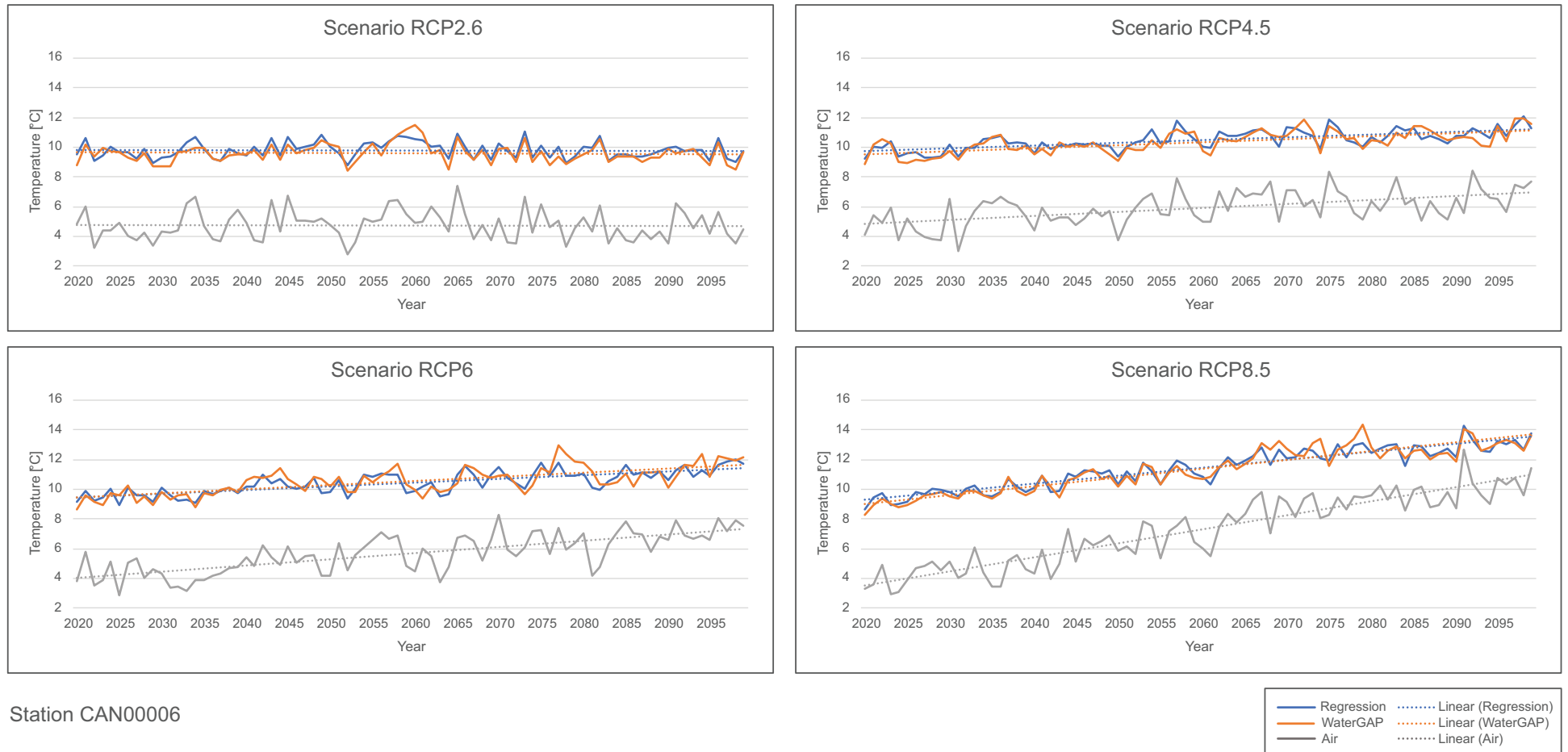


Figure 4.6.: A comparison of the scenarios RCP2.6, RCP4.5, RCP6 and RCP8.5 for the WaterGAP model without human use and power plant cooling and the regression model by PUNZET ET AL. (2012) between the years 2020 to 2099 for the station CAN00006.

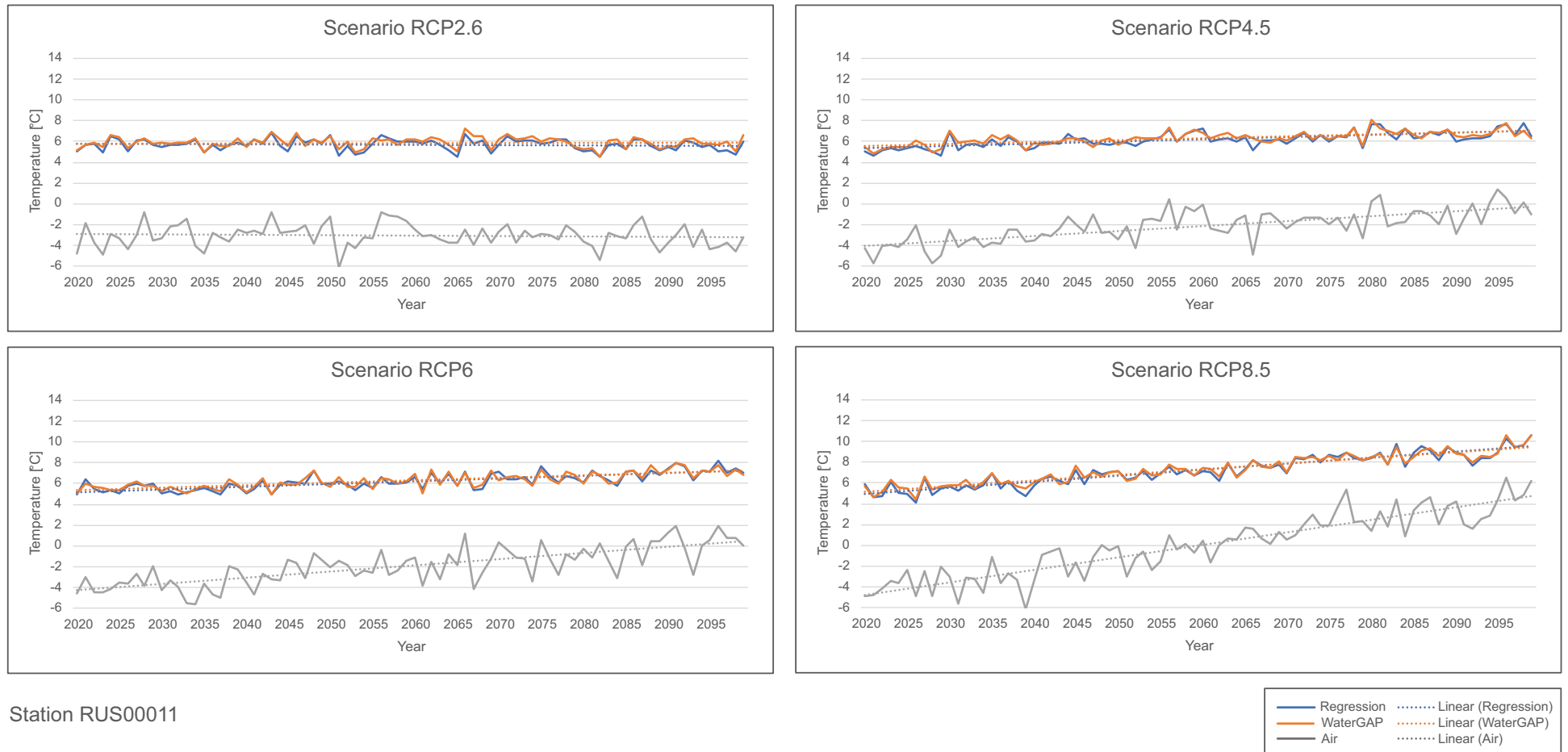
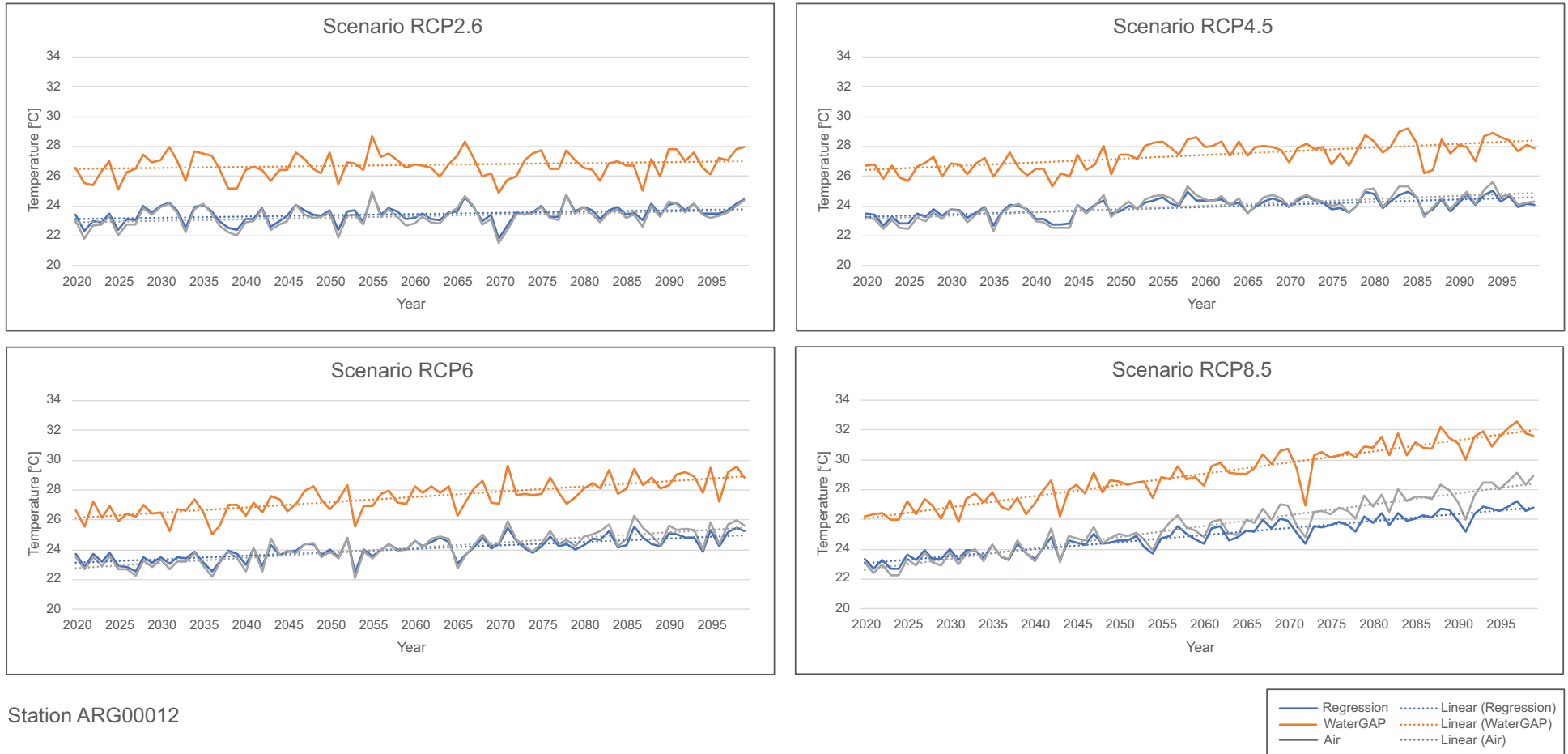


Figure 4.7.: A comparison of the scenarios RCP2.6, RCP4.5, RCP6 and RCP8.5 for the WaterGAP model without human use and power plant cooling and the regression model by PUNZET ET AL. (2012) between the years 2020 to 2099 for the station RUS00011.



Station ARG00012

Figure 4.8.: A comparison of the scenarios RCP2.6, RCP4.5, RCP6 and RCP8.5 for the WaterGAP model without human use and power plant cooling and the regression model by PUNZET ET AL. (2012) between the years 2020 to 2099 for the station ARG00012.

5. Conclusions and Prospects

Generally, the WaterGAP Model works well. The modeled data corresponds in nearly all evaluated geographic zones with the observed data. This can also be confirmed by comparing the WaterGAP modeled data with the regression model data by PUNZET ET AL. (2012), especially in Europe, Russia and North America. Nevertheless, there are some discrepancies. The geographic zones of Asia & Oceania, as well as South America, exhibit unsatisfactory results. The water temperatures are generally overestimated. Possible reasons are the water albedo, water emissivity, incoming radiation and the precipitation temperature as discussed in chapter 4.2. Most of the stations where WaterGAP indicates bad performance, the regression model also provides not satisfactory results. This indicates that the observed temperatures are off or some processes both models do not take into account are at play. Examples are the stations in Cambodia (KHM), India (IND) but also the swiss station CHE00001. One exception is the station AUS00004, where other problems of WaterGAP can be seen (see chapter 4.2). If there is too little water volume in the rivers and other surface water bodies or the catchment area is too small, the approach of VAN BEEK ET AL. (2012) in combination with WaterGAP comes to its limits.

Improvements should be possible in the ice formation calculation, especially for the conditions when the ice melts, breaks up and is transported downstream. Furthermore, the feedback of the ice formation to the channel roughness could be implemented, which is discussed in VAN BEEK ET AL. (2012). Also, the consideration of the power plant cooling water may be tweaked with real-world data of the water temperature fed back into the rivers. Further investigations could be made to determine a better assumption than the used value of +3 °C. The same could be said for the precipitation and surface runoff cooling. Perhaps three different values for the different climate regions of the world should be used. However, these last two assumptions have a minor influence on the results, as seen in the sensitivity analysis (see chapter 3.4). According to the sensitivity analysis, the groundwater temperature has the most impact on the results. Unfortunately, no real improvement can be made here.

The WaterGAP model upgraded with the water temperature calculation will definitely help the ISIMIP initiative in the future. Nevertheless, the climate change simulations show humankind will get into significant troubles if climate change progresses unhindered.

Bibliography

- VAN BEEK, L. P. H., T. EIKELBOOM, M. T. H. VAN VLIET & M. F. P. BIERKENS (2012): A physically based model of global freshwater surface temperature. *Water Resources Research*, 48(9), doi:10.1029/2012wr011819.
- CAISSIE, D. (2006): The thermal regime of rivers: a review. *Freshwater Biology*, 51(8), 1389–1406, doi:10.1111/j.1365-2427.2006.01597.x.
- DÖLL, P., F. KASPAR & B. LEHNER (2003): A global hydrological model for deriving water availability indicators: model tuning and validation. *Journal of Hydrology*, 270(1-2), 105–134, doi:10.1016/s0022-1694(02)00283-4.
- FADLI, K. I. E., R. S. CERVENY, C. C. BURT, P. EDEN, D. PARKER, M. BRUNET, T. C. PETERSON, G. MORDACCHINI, V. PELINO, P. BESSEMOULIN, J. L. STELLA, F. DRI-OUECH, M. M. A. WAHAB & M. B. PACE (2013): World Meteorological Organization Assessment of the Purported World Record 58°C Temperature Extreme at El Azizia, Libya (13 September 1922). *Bulletin of the American Meteorological Society*, 94(2), 199–204, doi: 10.1175/bams-d-12-00093.1.
- GOUDSMIT, G.-H., H. BURCHARD, F. PEETERS & A. WÜEST (2002): Application of k- ϵ turbulence models to enclosed basins: The role of internal seiches. *Journal of Geophysical Research: Oceans*, 107(C12), 23–1–23–13, doi:10.1029/2001jc000954.
- GUPTA, H. V., H. KLING, K. K. YILMAZ & G. F. MARTINEZ (2009): Decomposition of the mean squared error and NSE performance criteria: Implications for improving hydrological modelling. *Journal of Hydrology*, 377(1-2), 80–91, doi:10.1016/j.jhydrol.2009.08.003.
- HERBERT, C. & P. DÖLL (2019): Global Assessment of Current and Future Groundwater Stress With a Focus on Transboundary Aquifers. *Water Resources Research*, doi:10.1029/2018wr023321.
- ICAO (1993): Manual of the ICAO standard atmosphere extended to 80 kilometres (262 500 feet) = Manuel de l'atmosphère type OACI : élargie jusqu'à 80 kilomètres (262 500 pieds) = Manual de la atmósfera tipo de la OACI : ampliada hasta 80 kilómetros (262 500 pies), third edition, Montreal: International Civil Aviation Organization (ICAO).
- ICWRGC, (INTERNATIONAL CENTRE FOR WATER RESOURCES AND GLOBAL CHANGE). (n.d.): Global Freshwater Quality Database. Website.
URL: <<https://gemstat.org>> (last visit: 2020-08-16).

- JONES, C., M. SULTAN, E. YAN, A. MILEWSKI, M. HUSSEIN, A. AL-DOUSARI, S. AL-KAISY & R. BECKER (2008): Hydrologic impacts of engineering projects on the Tigris–Euphrates system and its marshlands. *Journal of Hydrology*, 353(1-2), 59–75, doi: 10.1016/j.jhydrol.2008.01.029.
- LANGE, J. (2009): *Wärmelast Rhein: Studie*, Mainz: Bund für Umwelt und Naturschutz Deutschland (BUND).
URL: <<https://www.bund-rlp.de/service/publikationen/detail/publication/studie-waermelast-rhein/>> (last visit: 2020-08-27).
- MATTHEWS, K. R. & N. H. BERG (1997): Rainbow trout responses to water temperature and dissolved oxygen stress in two southern California stream pools. *Journal of Fish Biology*, 50(1), 50–67, doi:10.1111/j.1095-8649.1997.tb01339.x.
- MÜLLER SCHMIED, H., D. CÁCERES, S. EISNER, M. FLÖRKE, C. HERBERT, C. NIEMANN, T. A. PEIRIS, E. POPAT, F. T. PORTMANN, R. REINECKE, M. SCHUMACHER, S. SHADKAM, C.-E. TELTEU, T. TRAUTMANN & P. DÖLL (2020): The global water resources and use model WaterGAP v2.2d: Model description and evaluation. *Geoscientific Model Development*, doi:10.5194/gmd-2020-225.
- MÜLLER SCHMIED, H., S. EISNER, D. FRANZ, M. WATTENBACH, F. T. PORTMANN, M. FLÖRKE & P. DÖLL (2014): Sensitivity of simulated global-scale freshwater fluxes and storages to input data, hydrological model structure, human water use and calibration. *Hydrology and Earth System Sciences*, 18(9), 3511–3538, doi:10.5194/hess-18-3511-2014.
- NASH, J. E. & J. V. SUTCLIFFE (1970): River flow forecasting through conceptual models part I — A discussion of principles. *Journal of Hydrology*, 10(3), 282–290, doi:10.1016/0022-1694(70)90255-6.
- OLDEN, J. D. & R. J. NAIMAN (2010): Incorporating thermal regimes into environmental flows assessments: modifying dam operations to restore freshwater ecosystem integrity. *Freshwater Biology*, 55(1), 86–107, doi:10.1111/j.1365-2427.2009.02179.x.
- OZAKI, N., T. FUKUSHIMA, H. HARASAWA, T. KOJIRI, K. KAWASHIMA & M. ONO (2003): Statistical analyses on the effects of air temperature fluctuations on river water qualities. *Hydrological Processes*, 17(14), 2837–2853, doi:10.1002/hyp.1437.
- PIK, (POTSDAM INSTITUTE FOR CLIMATE IMPACT RESEARCH). (n.d.): IPSL-CM5A-LR from the Inter-Sectoral Impact Model Intercomparison Project (ISIMIP). Website.
URL: <<https://www.isimip.org/gettingstarted/input-data-bias-correction/details/53/>> (last visit: 2020-08-16).
- PUNZET, M., F. VOSS, A. VOSS, E. KYNAST & I. BÄRLUND (2012): A Global Approach to Assess the Potential Impact of Climate Change on Stream Water Temperatures and Related In-Stream First-Order Decay Rates. *Journal of Hydrometeorology*, 13(3), 1052–1065, doi: 10.1175/jhm-d-11-0138.1.

- RITTER, A. & R. MUÑOZ-CARPENA (2013): Performance evaluation of hydrological models: Statistical significance for reducing subjectivity in goodness-of-fit assessments. *Journal of Hydrology*, 480, 33–45, doi:10.1016/j.jhydrol.2012.12.004.
- ROBARTS, R. D. & T. ZOHARY (1987): Temperature effects on photosynthetic capacity, respiration, and growth rates of bloom-forming cyanobacteria. *New Zealand Journal of Marine and Freshwater Research*, 21(3), 391–399, doi:10.1080/00288330.1987.9516235.
- RSTUDIO TEAM (2020): RStudio: Integrated Development Environment for R, Boston, MA: RStudio, PBC. **URL:** <http://www.rstudio.com/>.
- TOPRAK, Z. F. & M. E. SAVCI (2007): Longitudinal Dispersion Coefficient Modeling in Natural Channels using Fuzzy Logic. *CLEAN – Soil, Air, Water*, 35(6), 626–637, doi:10.1002/clen.200700122.
- VANDERKELEN, I., N. P. M. LIPZIG, D. M. LAWRENCE, B. DROPPERS, M. GOLUB, S. N. GOSLING, A. B. G. JANSSEN, R. MARCÉ, H. M. SCHMIED, M. PERROUD, D. PIERSON, Y. POKHREL, Y. SATOH, J. SCHEWE, S. I. SENEVIRATNE, V. M. STEPANENKO, Z. TAN, R. I. WOOLWAY & W. THIERY (2020): Global Heat Uptake by Inland Waters. *Geophysical Research Letters*, 47(12), doi:10.1029/2020gl087867.
- VAN VLIET, M. T. H., L. P. H. VAN BEEK, S. EISNER, M. FLÖRKE, Y. WADA & M. F. P. BIERKENS (2016): Multi-model assessment of global hydropower and cooling water discharge potential under climate change. *Global Environmental Change*, 40, 156–170, doi:10.1016/j.gloenvcha.2016.07.007.
- VAN VLIET, M. T. H., W. H. P. FRANSSSEN, J. R. YEARSLEY, F. LUDWIG, I. HADDELAND, D. P. LETTENMAIER & P. KABAT (2013): Global river discharge and water temperature under climate change. *Global Environmental Change*, 23(2), 450–464, doi:10.1016/j.gloenvcha.2012.11.002.
- VAN VLIET, M. T. H., J. R. YEARSLEY, W. H. P. FRANSSSEN, F. LUDWIG, I. HADDELAND, D. P. LETTENMAIER & P. KABAT (2012): Coupled daily streamflow and water temperature modelling in large river basins. *Hydrology and Earth System Sciences*, 16(11), 4303–4321, doi:10.5194/hess-16-4303-2012.
- WANDERS, N., M. T. H. VLIET, Y. WADA, M. F. P. BIERKENS & L. P. H. R. BEEK (2019): High-Resolution Global Water Temperature Modeling. *Water Resources Research*, 55(4), 2760–2778, doi:10.1029/2018wr023250.
- WANDERS, N. & Y. WADA (2015): Human and climate impacts on the 21st century hydrological drought. *Journal of Hydrology*, 526, 208–220, doi:10.1016/j.jhydrol.2014.10.047.
- WEEDON, G. P., G. BALSAMO, N. BELLOUIN, S. GOMES, M. J. BEST & P. VITERBO (2014): The WFDEI meteorological forcing data set: WATCH Forcing Data methodology

applied to ERA-Interim reanalysis data. *Water Resources Research*, 50(9), 7505–7514, doi: 10.1002/2014wr015638.

WMO (2017): *WMO Guidelines on the Calculation of Climate Normals*, Geneva: World Meteorological Organization (WMO).

YEARSLEY, J. R. (2009): A semi-Lagrangian water temperature model for advection-dominated river systems. *Water Resources Research*, 45(12), doi:10.1029/2008wr007629.

ZAMBRANO-BIGIARINI, M. (2020): *hydroGOF: Goodness-of-Fit Functions for Comparison of Simulated and Observed Hydrological Time Series*. Website.

URL: <https://CRAN.R-project.org/package=hydroGOF> (last visit: 2020-08-17).

A. Appendix

This master thesis has a digital appendix that contains all data and scripts created during the course of the thesis.

A.1. Structure of Folders

A.1.1. Folder evaluations

Subfolder Evaluation_GIS

ARCGIS projects used for evaluation of water temperature changes under climate change conditions (folder future), the map of cells where the river water temperature calculation is omitted (folder riverlength_hasOutflow) and the map of the locations of the stations used (stations).

Subfolder future_scenarios

Excel workbooks with data from the WaterGAP model and the regression model by PUNZET ET AL. (2012), as well as air temperatures for the period 2020 to 2099 from the climate forcing IPSL-CM5A-LR by ISIMIP. The subfolders contain the workbooks for the different scenarios RCP2.6, RCP4.5, RCP6 and RCP8.5. The subfolder meta contains the meta data used to create the workbooks.

Subfolder Scenarios

The following subfolders contain the evaluations of the different scenarios computed by WaterGAP in Excel workbooks.

GW_4deg

Calculated with reservoirs, power plant cooling (used water + 3 °C), ice formation, water use, groundwater temperature 4 °C. Rain temperature and surface runoff temperature are set to air temperature – 1.5 °C.

GW_10deg

Calculated with reservoirs, power plant cooling (used water + 3 °C), ice formation, water use, groundwater temperature 10 °C. Rain temperature and surface runoff temperature are set to air temperature – 1.5 °C.

GW_max_25deg

Calculated with reservoirs, power plant cooling (used water + 3 °C), ice formation, water use, groundwater temperature equals yearly mean air temperature with max. 25 °C. Rain temperature and surface runoff temperature are set to air temperature – 1.5 °C.

natural_run

Calculated as natural run. Power plant cooling (used water + 3 °C), water use and reservoirs are disabled. Reservoirs are treated as global lakes. Groundwater temperature equals yearly mean air temperature. Rain temperature and surface runoff temperature are set to air temperature – 1.5 °C. Ice formation is enabled.

no_ice

Calculated with water use, power plant cooling (used water + 3 °C) and reservoirs. Groundwater temperature equals yearly mean air temperature. Rain temperature and surface runoff temperature are set to air temperature – 1.5 °C. Ice formation is disabled.

no_reservoir

Calculated with water use, power plant cooling (used water + 3 °C) and ice formation. Groundwater temperature equals yearly mean air temperature. Rain temperature and surface runoff temperature are set to air temperature – 1.5 °C. Reservoirs are disabled and are treated as global lakes.

no_usage

Calculated with reservoirs, power plant cooling (used water + 3 °C) and ice formation. Groundwater temperature equals yearly mean air temperature. Rain temperature and surface runoff temperature are set to air temperature – 1.5 °C. Water use is disabled.

power_plants_30deg

Calculated with reservoirs, ice formation and water use, power plant cooling water discharge temperature is 30 °C. Groundwater temperature equals yearly mean air temperature. Rain temperature and surface runoff temperature are set to air temperature – 1.5 °C.

power_plants_plus5

Calculated with reservoirs, ice formation and water use, power plant cooling water discharge temperature is river water temperature + 5 °C. Groundwater temperature equals yearly mean air temperature. Rain temperature and surface runoff temperature are set to air temperature – 1.5 °C.

power_plants_plus10

Calculated with reservoirs, ice formation and water use, power plant cooling water discharge temperature is river water temperature + 10 °C. Groundwater temperature equals yearly mean air temperature. Rain temperature and surface runoff temperature are set to air temperature – 1.5 °C.

rain_no_cooling

Calculated with reservoirs, power plant cooling (used water + 3 °C), ice formation and water use. Groundwater temperature equals yearly mean air temperature. Rain temperature and surface runoff temperature are set to air temperature.

with_power_plants

This is the standard run calculated with reservoirs, power plant cooling (used water + 3 °C), ice formation and water use. Groundwater temperature equals yearly mean air temperature. Rain temperature and surface runoff temperature are set to air temperature – 1.5 °C.

without_power_plants

Calculated with water use, ice formation and reservoirs. Groundwater temperature equals yearly mean air temperature. Rain temperature and surface runoff temperature are set to air temperature – 1.5 °C. Power plant cooling is disabled.

Subfolder sensitivity_analysis

Sensitivity analysis for one station per geographic region. The evaluated parameters are the groundwater temperature, the precipitation and surface runoff temperature decrease and the power plant cooling water temperature increase. Data is available in Excel workbooks.

A.1.2. Folder model_data

These folders contain model data.

Subfolder IPSL-CM5A-LR_complete_timeseries

WaterGAP results for IPSL-CM5A-LR climate forcing

Subfolder punzet_regression_model_results

results of PUNZET ET AL. (2012) regression model for IPSL-CM5A-LR climate forcing

Subfolder punzet_regression_month_mean

air temperature as monthly mean for PUNZET ET AL. (2012) regression model for both climate forcings

Subfolder WFD_bc_WFDEI_timeseries_validation

all validation runs with WFD_bc_WFDEI climate forcing

A.1.3. Folder R_scripts

These scripts are used for this Master Thesis and are created by Sebastian Ackermann. U

A.1.4. Folder validation_data

This folder contains original zip-files of observed data downloaded from:

<https://gemstat.org/data/data-portal/>

A.2. Description of R Scripts

collect_all_ids.R

This script combines ArcID_CLM.txt and ArcID_GCRC.txt to ArcID_GCRC_CLM.txt. ArcID_GCRC_CLM.txt contains references between cell IDs of ARC (GIS), WaterGAP and CLM. The file is used in the scripts **regressiontemperature.R** and **regfuture2.R**.

meantemp.R

This script creates average monthly or yearly air temperatures from daily temperature files used in WaterGAP. The average monthly air temperatures are used to calculate Regression Model data after PUNZET ET AL. (2012).

This data is saved in the folder punzet_regression_month_mean and its subfolders. The average yearly air temperatures are used as groundwater temperatures for the water temperature calculation in WaterGAP. This data can be found on the server.

regfuture2.R

This script creates Excel workbooks with water temperatures from regression model and WaterGAP as well as air temperatures. The results of this script can be found in the folder /evaluations/future_scenarios and its subfolders.

regressiontemperature.R

This script creates binary files with regression model data after PUNZET ET AL. (2012). The data are calculated from monthly mean air temperatures created with the script **meantemp.R**.

temperatureValidation.R

This script creates an Excel workbook containing observed data and corresponding modeled data. The Nash-Sutcliffe Efficiency (NSE), the Root-mean-square deviation (RMSD) and the Kling-Gupta Efficiency (KGE) are calculated and written into the sheets, one per station.